INVESTIGATING SOLID ELECTROLYTES AND CATALYSTS FOR ELECTROCHEMICAL AMMONIA SYNTHESIS

By

Nicholas Hortance

Dissertation

Submitted to the Faculty of the

Graduate School of Vanderbilt University

in partial fulfillment of the requirements

for the degree of

DOCTOR OF PHILOSOPHY

in

Interdisciplinary Materials Science

August 12, 2022

Nashville, Tennessee

Approved:

David E. Cliffel, Ph.D.

Kelsey B. Hatzell, Ph.D.

Janet Macdonald, Ph.D.

Richard F. Haglund, Ph.D.

Joshua D. Caldwell, Ph.D.

Dedicated to my mother, Gina Hortance. The strongest, smartest, and most caring person I've ever known

ACKNOWLEDGMENTS

Throughout my academic journey, there have been people that have taken the time out of their day to help guide me toward my doctorate degree. First and foremost I would like to thank my advisors, Dr.Cliffel and Dr.Hatzell, for their mentoring and guidance, as well as for introducing me to a field of science that intrigues me endlessly. To my committee members, Dr.Haglund; Dr.Macdonald; and Dr.Caldwell, I would like to thank you for your insight and conversations that have led me to refine the way that I conduct research.

Prior to my studies in Vanderbilt, I was inspired by many teachers, professors, and staff from my highschool and at the University of Miami. To my highschool chemistry teacher, Dr.Trafton, I am grateful that you took notice of my interests in science and helped to teach me and others with excitement. To my university professor Dr. Ines Basalo, thank you for being an integral part in helping me to craft my applications, resume, and recommendations that led me to pursuing my PhD. To my undergraduate research advisor, Dr.Emrah Celik, I am really glad that you were the one to introduce me to research and had me contribute to many projects, which really boosted my confidence and cultivated my research interests. And to the office manager of mechanical engineering, Marisol Pernas, I thank you for treating me like family and for being invested in my future, as you helped me figure out my priorities and navigate undergraduate life.

In Vanderbilt, I have had the pleasure of working in two research groups, and this has led me to interact with so many colleagues that have helped me grow intellectually and socially. Thank you to Kris, Brice, Marm, Yanjie, and Wahid for particularly helping me get started in my first year as well as for the endless laughter and stories. To Matt, Katie, Yuxun, and Nicole, thank you for the much needed coffee sessions and discussions that kept me grounded (bad pun). To those that I met in the Cliffel lab, I thank you for including me in the group and making me feel welcome in the short time that I've been here. I would particularly like to thank Will and Aaron for the many lunch adventures and for helping me

navigate being an engineer in a chemistry world.

I would be remiss if I didn't mention those who have helped me transition into the Interdisciplinary Materials Science program. To Sarah Ross, Alisha Mccord and Dr.Walker I would like to say thank you for making the transition to graduate school as seamless as possible, a task that would not have been possible without you.

A special thanks is reserved for my mom, Gina Hortance, who always supported my dreams and ambitions, and for most importantly teaching me about God and the positive impact that I can have on society. I am also grateful to my sister Gianne and my dad Thierry for the emotional and financial support that you have given me when I need it the most. To my longtime friends Kevin; Qiwei; Lenin; and Anthony, I am pleased to have you all as friends who continue to uplift me and challenge me in all things. Thank you to my aunts, uncles, and cousins for the time we share together, and I look forward to many more opportunites to reconvene. I am happy and content to have you all as my family, and I hope to reciprocate the goodwill notions that you have shown to me.

TABLE OF CONTENTS

LIST OF TABLES

LIST OF FIGURES

CHAPTER 1

The Need for Sustainable Ammonia Production

*Portions of this chapter are reproduced from Fernandez *et al.* [24] with permission from the Royal Society of Chemistry

1.1 Introduction

Synthetic ammonia is a valuable commodity that has helped to shape the world we live in today. Its influence spans from enhancing agricultural practices (i.e. N-containing fertilizer) to producing explosive chemicals (e.g. nitroglycerin). Since the development of the Haber-Bosch process, both the amount of ammonia and global population have increased rapidly (Fig 1.1). It is theorized that without the Haber-Bosch process, the global population would be roughly 3 billion people short of the total 7 billion that exist today.[1] Cur-

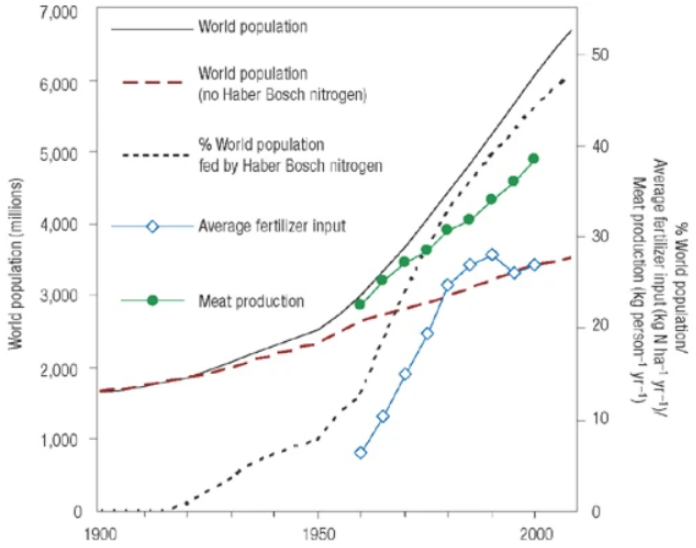

Figure 1.1: Of the total world population (solid line), an estimate is made of the number of people that could be sustained without reactive nitrogen from the Haber–Bosch process (long dashed line), also expressed as a percentage of the global population (short dashed line). The recorded increase in average fertilizer use per hectare of agricultural land (blue symbols) and the increase in per capita meat production (green symbols) is also shown; Reproduced with permission from Erisman *et al.* [1]

rently, 140 million metric tons of ammonia are produced annually using the Haber-Bosch process.[25] The process operates at elevated temperatures and pressures, and uses pure hydrogen as a feed source from steam reforming. At intermediate temperatures ($\approx 480^{\circ}$C) the kinetics of the standard K-promoted iron catalyst are decent for ammonia production, however, ammonia decomposition can occur at these temperature and thus high pressures ($\geq$150-300 bar)[26] are often employed to combat this effect. The subsequent conversion efficiency of N_2 to NH_3 for this process is 15% when considering a single pass.[27]

As pivotal as the Haber-Bosch process was to population growth, it is now regarded as unsustainable. Two percent of all of the world's energy supply is directed toward this process, while also accounting for 1% of the world's CO_2 emissions.[28] Additionally, these industrial plants are heavily centralized, and so rural communities have reduced access to this valuable chemical. These negative attributes motivate the need for alternative technologies that are sustainable and can decentralize the supply of ammonia.

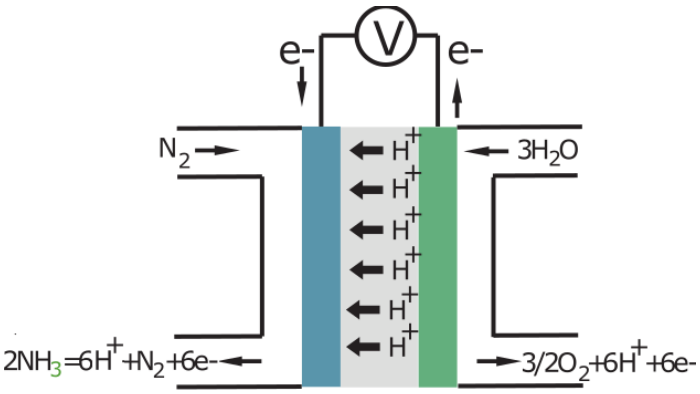

Figure 1.2: Electrochemical ammonia process employing nitrogen and water to form ammonia

An alternative approach to the Haber-Bosch process is electrochemical ammonia synthesis (EAS). In essence, an electrochemical cell consists of an anode, a cathode and an electrolyte. Based on the operating conditions of the synthesis, the cell will use either a solid-state, polymer, or aqueous electrolyte. Regardless, hydrogen/water is oxidized at the anode to form H^+ ions which migrate through the electrolyte to the cathode (Fig 1.2). Nitrogen is adsorbed at the cathode and is subsequently protonated from the previously

formed H^+ ions. This process is able to reduce the amount of energy needed to produce ammonia by implementing a voltage bias on the cathode (as opposed to using pressure as in industrial plants). Additionally, EAS is thermodynamically capable of producing ammonia using H_2O as a proton source as opposed to pure H_2, but this is not the case for industrial plants.[24,29] This alternative proton source can greatly reduce the amount of CO_2 emissions, since it would no longer rely on steam reforming.

Recently, a solid-state electrochemical cell successfully synthesized ammonia at intermediate temperatures (550-650 °C), ambient pressure, and using the same feed gasses as a typical Haber-Bosch plant.[30] For the same output of ammonia, the authors were able to decrease the amount of energy used by 25% and decrease the amount of CO_2 produced by 50% as compared to a Haber-Bosch plant. For the cathode material, they selected a vanadium based catalyst (VN-Fe) due to its reported high performance under room temperature studies. This illustrates that there is great progress in the development of electrochemical ammonia systems, and that they can be further studied by implementing better performing components.

Herein, the performance of solid-state electrolytes and catalysts are assessed for electrochemical ammonia synthesis. To properly discuss the performance of the solid-state electrolytes, Chapter 1 gives a thorough review of their functionality and performance. Chapter 2 then delves into an experimental study focused on implementing a proton conducting electrolyte. Thereafter, a sodium and potassium conducting electrolyte are studied in terms of their ability to electrochemically promote the ammonia synthesis reaction in a hydrogen deficient environment (Chapter 3). The final project (Chapter 4) investigates the surprising process of simultaneously reducing copper ions and synthesizing ammonia using a vanadium oxide-based catalyst in an H-cell device.

1.2 Review of Solid Electrolytes used for Intermediate Temperature Ammonia Synthesis

The central component of a solid-state electrolysis cell is the membrane electrode assembly, which is composed of two electrodes (anode and cathode) and a dense solid electrolyte. When a proton conducting electrolyte is employed, N_2 reduction and H_2/H_2O oxidation reactions occur separately at the cathode and anode (Fig. 1.3a). In contrast, N_2 reduction and H_2O dissociation occur at a single electrode (cathode) in the electrolysis cell with an oxygen ion-conducting electrolyte. Thus, oxygen ion-conducting electrolytes are challenging to implement and are fundamentally limited by the cathode electrocatalyst (detailed).

All components must exhibit chemical and mechanical stability at intermediate temperatures (200-650°C) to be viable for electrosynthesis. The anode and cathode electrodes are ideally porous to enable gas transport and comprise an inorganic mixed ion and electron conductor and an active catalyst (Fig. 1.3). The solid electrolyte must show high ionic conductivity, chemical compatibility with the catalyst, and negligible electronic conductivity.

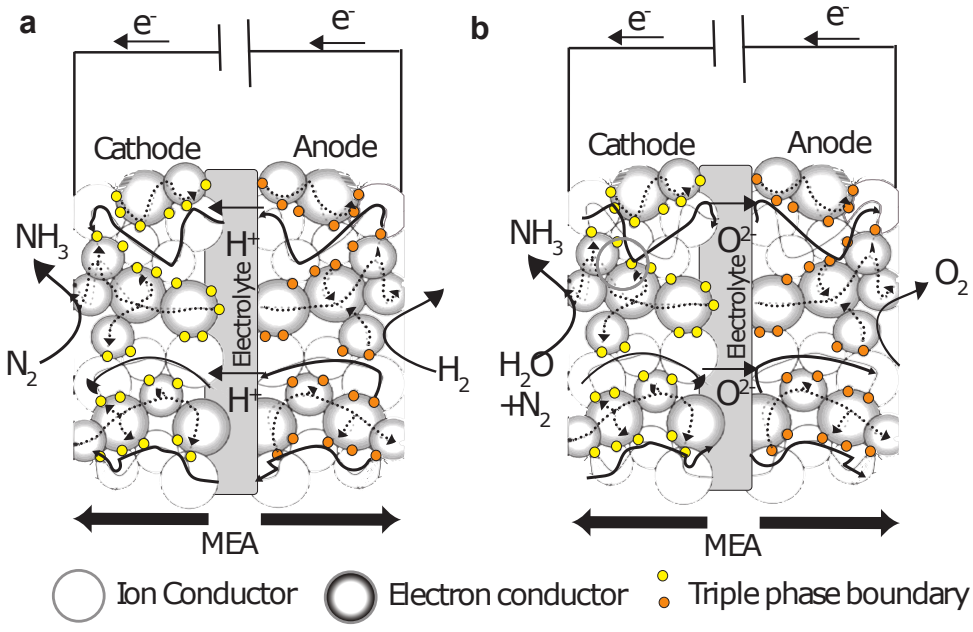

Figure 1.3: (a) Proton and (b) oxygen-ion conducting solid electrolytes have been investigated for intermediate temperature ammonia electrosynthesis cells.

Trace electronic conductivity in a solid electrolyte can decrease the transference number and current efficiency of a cell. Thus, material interactions between the catalyst, electrode, and electrolyte is immensely important for engineering durable solid oxide electrolysis cells.

The most common solid electrolytes used are proton, oxide ion, and nitride ion conductors. With the exception of oxygen conductors, the ions being conducted through the electrolyte may also serve as hydrogen or nitrogen sources for ammonia synthesis. Often, the solid electrolytes are made from ceramic based materials, and thus conductivity is heavily dependent on temperature (200 - 650°C). This is because of the relatively high activation energy for ion migration, leading to the need for elevated temperatures to overcome this barrier. The following sections discuss the use of solid state electrolytes design.

1.2.1 Proton Conducting Inorganic Electrolytes

Inorganic proton-conducting electrolytes are the most common solid-state electrolyte. There are three families of proton conducting electrolytes that are explored for intermediate temperature ammonia electrosynthesis: solid acids[31–34], oxides (perovskites, flourites, pyrochlores) (Fig.1.4)[2,35–38], and composite electrolytes (oxide/binary phosphates and oxide/ternary carbonates).

Solid acid electrolytes were first introduced in 2001 and operate between 100-300°C[39]. Common stoichiometries for solid acid electrolytes are $MHXO_4$, MH_2XO_4, and $M_3H(XO_4)_2$, where *M* can be Cs, Rb, K, Na, and/or NH_4, and *X* can be P, S, Se, and As. Fundamentally, this family of electrolytes is comprised of oxyanions (e.g. ${SO_4}^{2-}$, ${SeO_4}^{2-}$, etc.) that have hydrogen bonds coordinated with other oxygen sites.[32,40] As the operating temperature increases from 100 to 300°C a phase transition occurs which results in a more disordered structure, due to the rapid reorientation of XO_4^{2-} anion groups which enables more facile proton transport between neighboring anion groups.[32,40] Subsequently, the ionic conductivity increases by an order of magnitude.

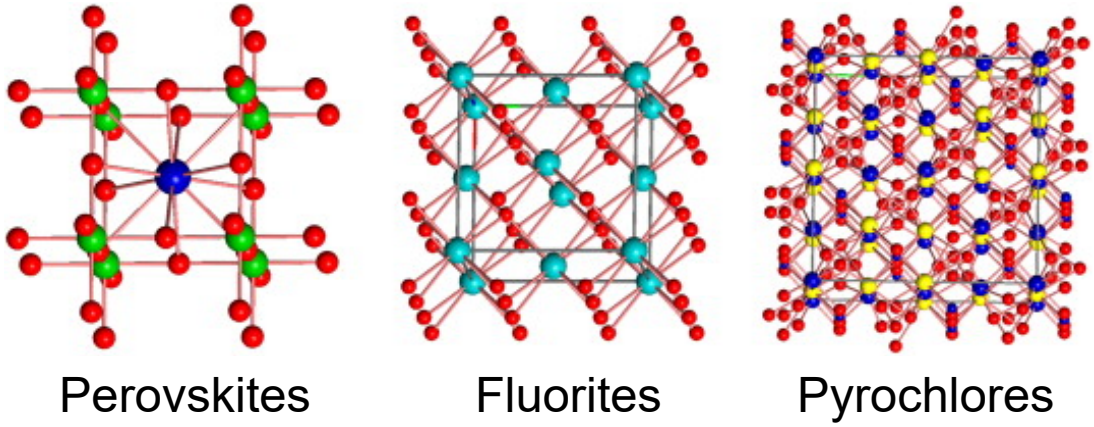

Figure 1.4: The primary solid electrolytes investigated for intermediate electrosynthesis of ammonia are: perovskites (green- B-site, blue- A-site, red- oxygen), fluorites (turquoise- metal site, red- oxygen) and pyrochlores (blue- B-site, yellow- A-site, red- oxygen); (Reproduced with permission[2], Elsevier).

One of the most promising solid acid electrolytes is CsH_2PO_4. This electrolyte transforms from a monoclinic to a cubic phase upon heating at $\approx$228°C and experiences a four-fold increase in the ionic conductivity ($>10^{-2}$ S cm^{-1})[41]. The melting temperature of a solid acid electrolyte can vary widely depending on the stoichiometry. One strategy employed to increase the melting temperature is the introduction of oxide (e.g. SiO_2) or pyrophosphate (SiP_2O_7)[42,43]. CsH_2PO_4/SiP_2O_7 composites form $CsH_5(PO_4)_2$ at the interfaces of the two materials which leads to higher ionic conductivities at lower temperatures. Furthermore, this composite demonstrates a nearly constant ionic conductivity ($\geq$ 20 mS cm^{-1}) between 100 to 270°C[9,43] (Fig. 1.5). Finally, the addition of SiP_2O_7 reduces the plasticity of the solid electrolyte which enables more compliant interfaces and less short-circuiting.[41]

Recently, a wide-range of solid acid electrolytes (e.g. $CsHSO_4$[44]; $Rb_3H(SeO_4)_2$[45]; and $(NH_4)_3H(SO_4)_2$[46]) have been explored for electrosynthesis of ammonia. A significant challenge with solid acid electrolytes is electrolyte decomposition when in contact with a base (e.g. NH_3). One solution explored in the literature is the use of a proton conducting barrier film (e.g. AgPd), coated directly onto a CsH_2PO_4/SiP_2O_7 solid electrolyte. The

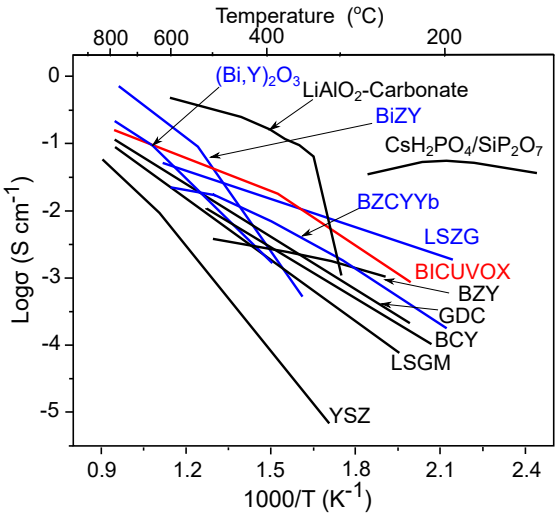

Figure 1.5: Ionic conductivity of common electrolytes (O^{2-} and H^{+} conductors) that have or have not yet been used for ammonia synthesis; $(Bi,Y)_2O_3$, $LiAlO_2$-Carbonate[3]: $LiAlO_2$-$(Li,Na,K)_2CO_3$, BZY: $BaZr_{0.8}Y_{0.2}$, LSZG[4]: $Li_{13.9}Sr_{0.1}Zn(GeO_4)_4$, BICUVOX[5]:$Bi_2V_{1.9}Cu_{0.1}O_{5.35}$,GDC[6]:$Ce_{0.9}Gd_{0.1}O_{1.95}$, LSGM[5]: $La_{0.9}Sr_{0.1}Ga_{0.8}Mg_{0.2}O_{2.85}$, YSZ[7]: $8\%Y_2O_3/ZrO_2$, BCY[8]:$BaCeO_3$, $Cs_2H_2PO_4/SiP_2O_7$[9], BZCYYb[10]: $BaZr_{0.4}Ce_{0.4}Y_{0.1}Yb_{0.1}$. Blue: H^{+} conducting electrolytes not yet used for ammonia synthesis; Red: O^{2-} conducting electrolytes not yet used for ammonia synthesis; Black: Electrolytes previously used for ammonia synthesis

barrier film mitigates acid/base interactions, enables proton transport, and allows for the use of dry gases (e.g. H_2)[47,48]. A faradaic efficiency around 2.6% was achieved using a barrier film. Another study examined a barrier-free CsH_2PO_4/SiP_2O_7 electrolyte with a range of noble-metal catalysts and could only achieve faradaic efficiencies $\sim$0.15%. In the absence of a barrier, it is necessary to utilize humidified gases to avoid dehydration[9]. Overall, the faradaic efficiency and synthesis rate were shown to decrease at voltages greater than 0.3V. At low voltages (0.15V) all catalysts (except Ru) showed similar synthesis rates of $0.8x10^{-10}$ mol $cm^{-2}s^{-1}$ at 220°C[9]. A wide range of side reactions can occur at elevated voltages including (1) the electrolyte decomposition at the catalyst|electrolyte interface and (2) the formation of hydrogen gas. Thus, low electrosynthesis voltages are desirable to avoid side reaction and achieve high energy efficiency in solid acid electrolytes.

The second family of electrolytes being explored for intermediate temperature ammonia

electrosynthesis are oxide solid electrolytes. Three prominent proton conducting oxides include: (1) perovskite, (2) flourite, and (3) pyrochlore (Fig. 1.4). Proton transport in oxides primarily occurs through the Grotthuss mechanism which involves proton hopping between neighboring oxygen atoms[49,50]. Transport properties can be tuned via increasing the concentration of protonic defects (e.g. OH^- or oxyanions)[51]. Tuning the defect chemistry via elemental doping is one strategy often employed to increase the oxygen vacancy concentration[32,40]. These solid electrolytes typically operate between 400 and 650°C. Thus, the operating temperature is similar to the Haber-Bosch and can even exceed it at times. Thermodynamically, ammonia decomposition at these temperatures is possible as discussed in Section 2, and should be avoided.

The ion in the electrolyte can act both as a charge carrying element and as a catalytic promoter. The mobile ion in the electrolyte can dynamically alter the electronic structure of the catalyst and influence the binding energies of the reactant and/or adsorbed molecules[52–54]. This phenomena is known as non-Faradaic electrochemical modification of catalytic activitiy (NEMCA)[55,56] or electrochemical promotion of catalysis (EPOC)[57,58]. Thus, control over transport within the electrolyte and at the electrolyte|electrode interface may provide a pathway toward controlling adsorbates and reaction kinetics.

Perovskites have the general form ABO_3, where *A* is typically Ba, Sr, Ca and/or La and *B* is either Ce or Zr. Oxygen vacancies in perovskite oxides determine material structures and properties such as ionic charge transport. The concentration of oxygen vacancies can be increased via doping the *B*-site with aliovalent cations such as yttrium or ytterbium. Perovskites with cerium ions in the *B*-site demonstrate a high ionic conductivity due to its exceedingly negative hydration enthalpy (e.g. -162.2 kJ/mol for $Ba(Ce_{0.9}Y_{0.1})O_{3-\delta}$[59]). Hydroxyl terminating groups can be retained at high temperatures when the hydration enthalpy becomes increasingly negative[60]. However many bulk electrolytes that have cerium atoms in the lattice are chemically unstable due to the formation of carbonates (e.g. as in the case of $BaCeO_3$ and $SrCeO_3$)[32,51]. Thus, zirconium and yttrium are doped into the

B-site of these cerates to promote stability.[36]

Early work using a perovskite, proton-conducting strontia-ceria-ytterbia (SCY) electrolyte ($SrCe_{0.95}Yb_{0.95}O_3$), explored ammonia decomposition during ammonia synthesis at elevated temperatures ($\geq$500°C)[56]. At 750°C, using symmetric Pd electrodes, a synthesis rate $\sim$4.8x10^{-9} mol $cm^{-2}s^{-1}$ was achieved. Furthermore, ammonia decomposition was shown to decrease at these high temperatures due to the NEMCA effect. In particular, proton 'spillover' can spread on the metal catalyst and form dipoles which decreases the catalyst potential. In this particular work, this led to a decrease in the binding strength of the catalyst to electron donating adsorbates such as NH_3[56,61]. The latter effect is attributed to the decrease in ammonia decomposition. In a follow up study, contrary results were observed for a SCY electrolyte coupled with Ag catalysts. This system experienced increases in ammonia decomposition upon applying a constant current[62]. These results suggest that the nature of the triple boundary and local electric field may play a role on the local binding energy. Additional investigations have been conducted using an SCY electrolyte with catalysts (e.g. Ag, AgPd) with little improvement to the synthesis rate[37,62,63]. Low synthesis rates have been attributed to low ionic conductivity and high ohmic resistances in SCY(Fig. 1.5).

Alternatively, there has been a significant interest in highly conducting $BaCeO_3$-based and $BaZrO_3$-based perovskite solid electrolytes. To improve the ionic conductivity the *B*-site is doped with yttrium to produce the commonly known BCY and BZY solid electrolytes. Yttrium doping introduces additional oxygen vacancies to the structure, which provides more pathways for protons to hop. $BaCe_{0.85}Y_{0.15}O_{3-\delta}$ (BCY) was implemented in a symmetric AgPd cell and obtained ammonia at a rate of 2.1×10^{-9} mol $cm^{-2}s^{-1}$ and efficiency above 60% at 500°C in a humidified hydrogen environment.[64] The transference number of protons with the structure (i.e fraction of current for protons relative to the total current) was near unity, but began to decrease as the applied current exceeded 12 mA cm^{-2}. This phenomenon was attributed to polarization of the electrode and a reduced

concentration of protons at the interface between the electrolyte and electrocatalyst. This however did not affect the synthesis rate since the optimal current density was found to be 0.75 mA cm^{-2}. Barium cerates (e.g. BCY) are chemically unstable with acidic reactants, while barium zirconates are known to be more stable. Table 1 summarizing the performances properties for a range of BZY and BCY electrolytes tested for electrosynthesis of ammonia.

Fluorite (AO_2) and pyrochlore ($A_2B_2O_7$) structured proton conductors are also used for ammonia electrosynthesis. Fluorite structured electrolytes have oxygen ions in cubic packing and tetravalent metal cations in alternating cube centers (Figure 1.4). Pyrochlores have an ordered defective fluorite structure where the *A* and *B* atoms are trivalent and tetravalent cations, respectively. Previously a AgPd—$La_{1.9}Ca_{0.1}Zr_2O_{6.95}$—AgPd cell synthesized ammonia at a rate of 2×10^{-9} mol $cm^{-2}s^{-1}$ and had a faradaic efficiency of 80% at 500°C using hydrogen and nitrogen.[65] Calcium doping causes the grains to enlarge and increases the grains and the grain boundary ionic conductivity.

The final type of proton conducting solid electrolyte being studied in ammonia electrosynthesis are composite electrolytes. These electrolytes combine two different types of ion conducting media and may actually have multiple charge carriers (i.e. H^+ and N^{3-}): (1) oxide and (2) phosphates or carbonates[3,66–68]. Combining multiple ion conductors together can enable tunable material properties (e.g. transport, thermal, mechanical, and/or electrical) (Fig. 1.5). Ternary, carbonate-based composite electrolytes commonly use $(Li,Na,K)_2CO_3$ because it has a relatively low melting point (396°C) and can achieve ionic reasonable ion conductivities (100 mS cm^{-1}) at 400°C[69]. Recently, a ceria-$Ca_3(PO_4)_2$-K_3PO_4 electrolyte was used to synthesize ammonia, where the hydrogen source was natural gas[66,67]. A synthesis rate $\sim$6.95x10^{-9} mol $cm^{-2}s^{-1}$ was achieved at 650°C. Interestingly, this electrolyte saw increases in ammonia synthesis rate as the temperature increased from 400 to 650°C, suggesting that ammonia decomposition was not affected by the temperature increase. However, in another study using a $LiAlO_2$-carbonate elec-

trolyte with a AgPd anode and a Fe_3Mo_3N-Ag cathode synthesized ammonia at a rate of 1.88×10^{-10} mol $cm^{-2}s^{-1}$ with a Faradaic efficiency of 1.84% at 425°C. In this study the rate and efficiency decreased as the temperature increased, suggesting ammonia decomposition played a role. Thus, the nature of ammonia decomposition in these mixed material systems are not well understood. Composites may be a pathway forward to tailor interfaces for either chemical stability or directed transport.

1.2.2 Proton Conducting Polymer Electrolytes

Proton conducting polymer electrolytes such as perfluorosulfonic acid (e.g. Nafion) are typically used in ambient, low temperature electrosynthesis. However, Nafion is operationally limited to ≤ 90°C since it fails retain moisture well above this temperature;[70,71] and recent studies suggest that they may not be suitable because it has a tendency to absorb ammonia resulting in accelerated decomposition of Nafion.[72] Despite the lack of studies, intermediate temperature synthesis of ammonia could benefit from using polymer electrolytes. High-temperature, polymer electrolyte membranes (HT-PEMs) are capable of operating within 100 to 200°C without the need of humidification (as is the case for Nafion). Phosphoric acid doped polybenzimidazole (PBI) is a well-known high temperature membrane investigated for its use in H_2/O_2 fuel cells, wherein it attains a power density within 500 - 800 mW/cm^2 at 100 to 200°C in a hydrogen/air mixture.[73] By comparison, solid oxide fuel cells attain power densities near 100 mW cm^{-2} at 350°C and 1400 mW cm^{-2} at 700°C.[74,75] However, steam cannot be used as a hydrogen source with PBI electrolytes because it will cause a loss in phosphoric acid groups. A more promising polymer is the SnP_2O_7/Nafion composite, which attains a high ionic conductivity of 100 mS cm^{-1} at 200°C, a similar power density of 800 mW cm^{-2}, and is stable in dry and wet conditions for over 1400 hours.[76] Polymer electrolytes that can sustain higher temperatures represent a very promising area for growth because scalable manufacturing methods are available. However to date there have been limited investigations that have been reported.

1.2.3 Oxygen Conducting Ceramic Electrolytes

An alternative to proton conducting electrolytes are oxide ion conducting electrolytes. The charge carrier (i.e. oxide ion) does not react in either the anode or cathode half cell reactions. Instead, steam and nitrogen are reactants at the cathode and are reduced to form ammonia. The two half-cell reactions that occur in a fuel cell configuration, operating with an oxide conducting electrolyte are (Fig. 1.3b):

$$3H_2O + N_2 + 6e^- \rightarrow 3O^2- + 2NH_3 \tag{1.1}$$

$$3O^{2-} \rightarrow \frac{3}{2}O_2 + 6e^- \tag{1.2}$$

Yttrium stabilized zirconia (YSZ), is a common oxide-conducting electrolyte comprised of 8%Y_2O_3/ZrO_2. Previously, a double-chamber set-up with a Ag|YSZ|Ru-Pd cell, demonstrated a synthesis rate of 1.5x10^{-13} mol $cm^{-2}s^{-1}$ at 650°C, with steam and nitrogen reactants.[77] The synthesis rate increased to nearly 7.5x10^{-13} mol $cm^{-2}s^{-1}$ as the temperature increased from 550 to 650 °C. Another study using a symmetric Pt|GDC|Pt cell utilized a more conductive electrolyte, i.e. gadolinium doped ceria (GDC), and achieved a higher formation rate on the order of 10^{-11} mol $cm^{-2}s^{-1}$ at 600°C.[78] The low synthesis rates may be attributed to using water vapor as a hydrogen source. The synthesis rate was shown to increase significantly with the use of hydrogen to 10^{-9} mol $cm^{-2}s^{-1}$ at 650°C using $Ce_{0.8}M_{0.2}O_{2-\delta}$ (doped with M=Gd, La, Y, or Sm)[79]. However, in this instance the doped cerates acted as proton conductors as opposed to oxygen conductors. Thus, the selection of H_2 or H_2O as a hydrogen source is non-trivial for both proton conducting and oxide conducting systems. Additionally, the $Ce_{0.8}M_{0.2}O_{2-\delta}$ doped cerates demonstrated a positive correlation between the ionic conductivity and the synthesis rate, further emphasizing the need for highly conductive electrolytes. Since oxygen and oxygen anions do not participate in the reaction mechanism for ammonia formation, a higher electrolyte conductivity should not adversely affect the faradaic efficiency. Recently, there have been numerous solid ion

conductors which have been discovered that can effectively operate at lower temperatures. $Bi_2V_{1.9}Cu_{0.1}O_{5.35}$ (BiCuVOX) is an example of an electrolyte which can operate at 400°C with conductivities near 10^{-2} S cm^{-1}(Fig. 1.5).

1.2.4 Conclusion

Ammonia is a key component in society today to sustain our population, which means that solving the sustainability issue of the Haber-Bosch process is of great importance. Solid-state electrochemical devices is one avenue of research that can reduce the energy consumption to produce ammonia, but appropriate materials selection remains a key part to making an efficient device. The review presented in this chapter offers a glimpse of the field of solid-state devices, particularly looking at the form and function of solid-state electrolytes. Since proton conductors are the most common type of electrolyte that also operates under milder conditions than oxygen ion conductors, a new proton conductor ($BaZr_{0.4}Ce_{0.4}Y_{0.1}Yb_{0.1}O_3$) was investigated in Chapter 1 for the purpose of synthesizing ammonia.

CHAPTER 2

Implementing a H^+ Conductor for Electrochemical Ammonia Synthesis

As mentioned in Chapter 1, proton conductors are a class of solid-state electrolytes that are most commonly used for ammonia synthesis since they can transfer protons as opposed to oxygen ions (as used in solid oxide fuel cells). While there is considerable interest in producing ammonia at ambient conditions using liquid and polymer cells, these systems typically suffer in terms of their efficiency. Several theoretical studies highlight the importance of using a non-aqueous electrolyte for enhanced selectivity, since they can aid in decreasing the hydrogen evolution reaction (HER).[80] Inorganic solid electrolytes that can operate at elevated temperatures and ambient pressure present a possible path forward to sustainable ammonia production.

Proton conductors permit diffusion of hydrogen ions by way of oxygen vacancies ($V_o^{\cdot\cdot}$), oxygen sites (O_x), and hydrated oxygen sites ($OH^{\cdot}$) in perovskite (ABO_3) inorganic materials. This type of structural diffusion is referred to as the Grotthuss mechanism, in that protons hop from oxygen site to oxygen site. Aliovalent dopants are typically used to enhance the conductivity of these electrolytes, as they can increase the concentration of oxygen vacancy sites. Examples of this include the doping of barium cerates and zirconates (BCY and BZY) using yttrium (Y^{3+}) and ytterbium (Yb^{3+}) ions, which act as substitutional atoms for cerium and zirconium sites respectively.

In this section, the proton conductor $BaZr_{0.4}Ce_{0.4}Y_{0.1}Yb_{0.1}O_3$ (BCZYYb4411) was implemented as an electrolyte for electrochemical ammonia synthesis. This electrolyte was chosen for its high ionic conductivity, stability in reducing and oxidizing environments, and due to it containing known catalytic promoter elements (Ba and Ce). Different conditions are implemented in the attempt to increase the resulting concentration of ammonia. The different parameters tested include temperature, test duration, gas com-

position, applied potential, and geometric area for the cathode. The performance of this electrolyte was compared with other electrolytes in literature, and recommendations are given as to how the field can progress with better experimental practices.

2.1 Methods

2.1.1 Electrolyte Synthesis

The proton conductor was synthesized using a solid-state reaction approach. Stoichiometric quantities of barium carbonate, zirconia, ceria, yttria, and ytterbium oxide precursors are ball-milled (PULVERISETTE 7 premium line, Fritsch) with zirconia balls and 15 mL of isopropyl alcohol for 16 hours. The homogenized mixture was dried at 80°C overnight and subsequently sieved (No. 170). Green pellets (i.e. intermediary pellets) are calcined in air at 1400°C for 10 hours with a 5 °C heating/cooling rate. Finally, the green pellets are crushed back into powder form for further sample preparation and characterization. The crystal structure and lattice constant of the electrolyte was determined by using x-ray diffraction (XRD) using a Cu K-α radiation source.

2.1.2 Ionic Conductivity

The protonic conductivity of the ceramic electrolyte is sufficient to ascertain the performance of the electrolyte in supplying protons to the cathode. In order to evaluate this conductivity, highly dense samples of the electrolyte are prepared along with electrodes adhered on either end. The electrolyte pellets are produced with an isostatic pressure of 400 MPa and sintered at 1600°C for 24 hours to form dense (>95%) samples. They are then polished using 600 and 1200 grit SiC paper sequentially. Silver paste (SPI supplies) was painted on both sides of the electrolyte along with silver leads, dried on a hot plate @ 50°C, and finally calcined at 900°C. The impedance was measured using a potentiostat/-galvanostat within 1 MHz and 0.5 Hz in a humidified atmosphere (from 300°C to 600°C) so as to increase the protonic defects, thereby illustrating the true protonic conductivity. The impedance of the bulk electrolyte was then evaluated using equivalent circuit fitting,

which was then implemented in the established Arrhenius equation to calculate the ionic conductivity.

2.1.3 Ammonia Synthesis

Symmetric cells, comprised of silver paladium electrodes (AgPd), were systematically evaluated for ammonia production. AgPd electrodes were chosen due to their relatively high affinity for hydrogen adsorption, which would benefit the dissociation of water at the anode and subsequent oxidation of hydrogen adatoms to form protons. So AgPd, paste is painted (3mm or 10mm diameter) onto the polished electrolyte surface, and the samples were subsequently dried in a vacuum oven at 60°C. Silver paste was then applied as a current collector to the AgPd electrodes and dried at room temperature. The ammonia tests occur in a double chamber reactor to separate the reduction/oxidation reactions (Figure 2.1). This was done by adhering the electrochemical cell to the top of the inner-chamber, alumina tube using a high-temperature sealing agent. The high temperature sealing agent (Ceramabond 552, Aremco) forms a hermetic seal, which effectively separates the reactant gases. The reactor was then placed into a tube furnace and heated at 600°C for 1 hour to set the sealing agent and calcine the electrodes.

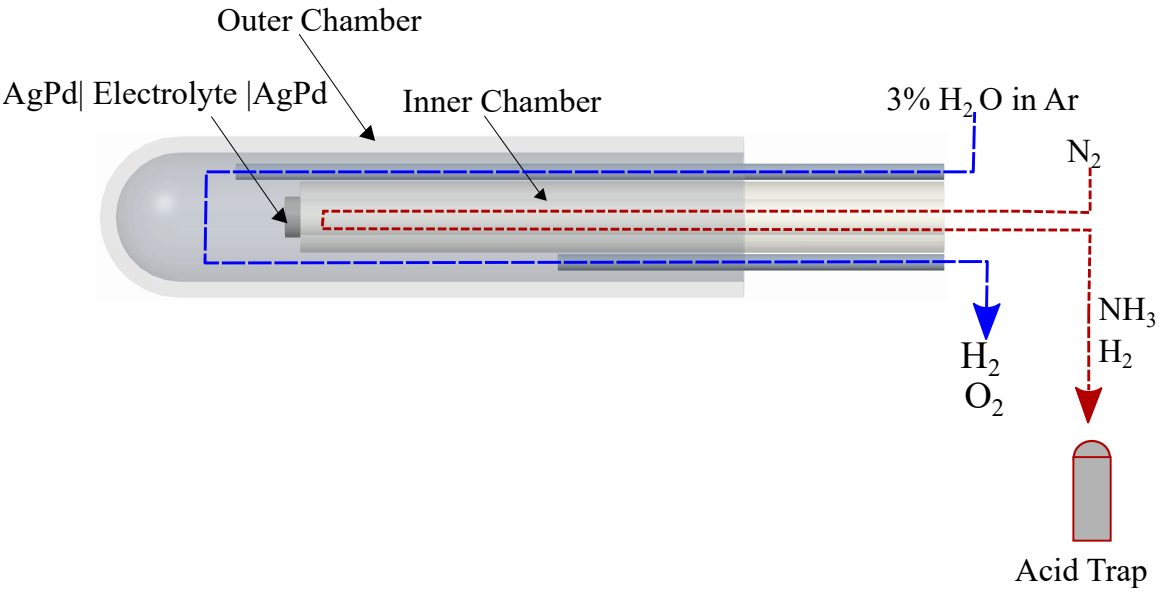

Figure 2.1: Double Chamber setup

Two different reactants were tested at the cathode: dry nitrogen gas and 3%H_2/N_2 gas, whereas humidified argon (3% H_2O) consistently flows in the anode throughout all the experiments. %, each with a flow rate of 115 sccm. %For the control and test experiments, a constant voltage potential of 0.8 V is applied using chronoamperometry for minutes. The subsequent effluent gasses emminating from the cathode flow into an acid trap (1 mM H_2SO_4), thereby converting ammonia into ammonium ions. The concentration of ammonia produced was then evaluated by converting the ammonium ions into indophenol, which is a chromataphore, and then using spectrophotometric detection.

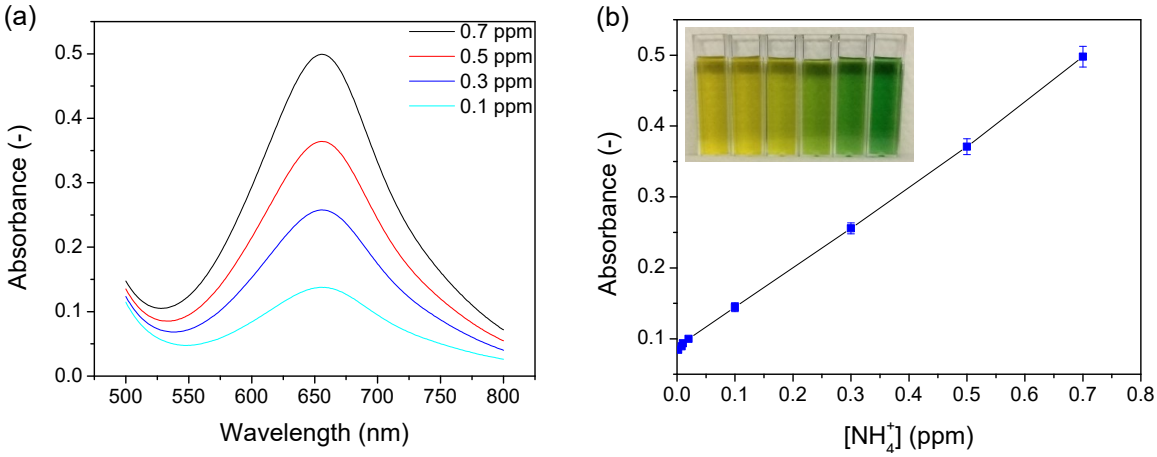

Figure 2.2: (a) Spectrophotometric response of indophenol (b) Corresponding calibration curve acquired from peak values of spectrophotometric response

The indophenol method follows the Berthelot reaction, in which ammonia reacts with a phenolic compound and hypochlorite along with a catalyst. A citrate buffer is also added to the solution to stabilize the pH. To quantify the concentration of ammonia obtained from a given experiment, a calibration curve was developed by plotting the absorbance obtained from a spectrophotometer at 655 nm for known concentrations of ammonium chloride (Figure 2.2). Control experiments are implemented to account for ambient sources of ammonia by using argon gas. A blank sample serves as a baseline for all tests and controls, and this sample undergoes all the steps of producing indophenol without any deliberate concentration of ammonia present. Additional controls consist of measuring ammonia in the argon gas tank, inside the reactor as argon flows through it at open circuit voltage (OCV),

and inside the reactor as argon flows through it at 0.8V. Valid tests are considered to be concentrations of ammonia that surpass the controls. Besides the controls produced with argon, the concentration of ammonia inside the nitrogen tank at OCV are also obtained. To determine the concentration of ammonia due to electrochemical synthesis, the experiments run at OCV are subtracted from the final amount to account for catalytically produced ammonia. The subsequent rate and efficiency metrics are evaluated using the following equations:

$$Rate = \frac{([NH_4^+{}_{Volt}] - [NH_4^+{}_{OCV}]) \cdot V}{t \cdot A} \tag{2.1}$$

$$\eta(\%) = \frac{3 \cdot F \cdot Rate}{I} \cdot 100 \tag{2.2}$$

Where, Rate is the rate of ammonia produced in mol/cm^2·s; $NH_4^+{}_{Volt}$ is the ammonium ion concentration after applying voltage to the cell (moles/L); $NH_4^+{}_{OCV}$ is the ammonium ion concentration taken at open circuit voltage (moles/L); V is the volume (L); t is the duration of the experiment; A is the geometric area of the electrode; η is the faradaic efficiency (%); F is faraday's constant; and I is the current density (A/cm^2).

2.2 Results and Discussion

2.2.1 Electrolyte Characterization

The diffraction pattern of the synthesized BZCYYb4411 powders corresponded to a cubic Pm3m space group and lattice constant of 4.28 Å. A lattice constant of 4.31 Å was obtained by Choi et al.[10] which indicates that there is just a slight discrepancy in volume between the two electrolyte. This could be due to the loss of barium during the solid state synthesis process that can lead to a reduction in the cell volume. This smaller volume could potentially influence the diffusion of protons through the electrolyte.

Further characterization of the electrolyte demonstrated the impedance of the electrochemical cell when in a humidified atmosphere (Figure 2.4a). The Nyquist plot has two characteristic semicircles that appear when the cell operated at 400, 500 and 600^{o}C,

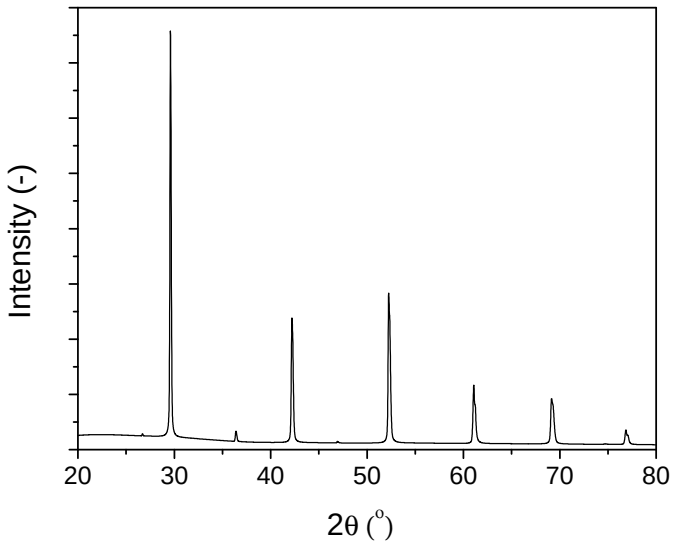

Figure 2.3: XRD of BZCYYb4411 electrolyte powder

which correspond to the bulk electrolyte resistance at high frequencies, and the electrode at lower frequencies. At temperatures lower than 300^{o}C, only a single semicircle is present at high frequencies along with a tail-end attributed to diffusion. With polycrystalline solid-electrolytes, grain boundary resistance may be influential at temperatures typically lower than 300^{o}C, which would entail that it has a higher resistance than the grains themselves. This theory is known as the 'brick-layer model'[81]; and so if the grain boundary resistance is higher than the grains, then a secondary semicircle will be present at these lower temperatures. Since this was not seen in the Nyquist plots at temperatures lower than 300^{o}C, the grain boundary resistance was assumed to be negligible. The resulting ionic conductivity is shown in Figure 2.4b; and although it is slightly smaller than that obtained in literature for this electrolyte[10], it is still amongst the highest ionic conductivities achieved by proton conductors.

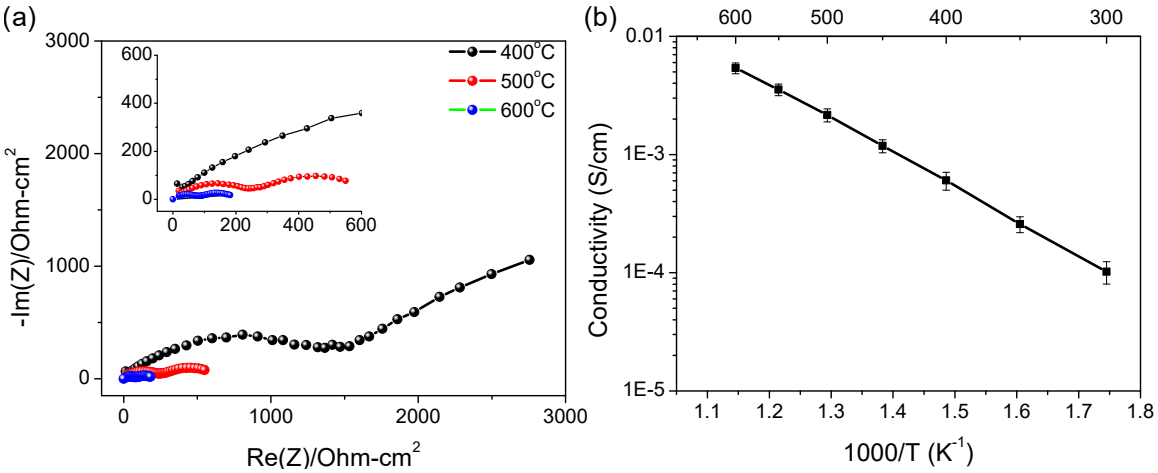

Figure 2.4: (a) ASR of Ag-symmetric cells at 400, 500 and 600^{o}C (b) Ionic conductivity of electrolyte within 300 and 600^{o}C

2.2.2 Ammonia Synthesis

2.2.2.1 Operating in Dry N_2

When the gas composition at the cathode consists of dry nitrogen gas, the synthesis of ammonia is entirely dependent on hydrogen ion pumping by the electrolyte to facilitate the proton/electron coupled reaction. Under this condition, we can test the efficacy of the electrolyte to pump protons stemming from the humidified argon source supplied at the anode. A working electrode diameter of 10mm was used under these conditions. When the reactor operates at 0.8V within 25 to 30 minutes (Table 2.1) then ammonia was synthesized at a maximum rate of 4.52x10^{-12} mol/cm^2·s with a maximum efficiency of 2.18%. To date, all of the reported literature results on electrochemical ammonia synthesis using dry nitrogen and steam are shown in Table 2.2. The experimental results in this study tested for 25 and 30 minutes correspond well with the literature results, especially considering that this study takes into account background sources of ammonia as opposed to those in literature.

Temperature (°C)	**Voltage (V)**	**Duration (hours)**	**Current Density (mA/cm^2)**	**Rate ($mol/cm^2 \cdot s$) x10^{-12}**	**Faradaic Efficiency (%)**
450	0.8	0.5	0.12	4.52	2.18
	0.8	0.42	0.18	2.3	0.37
	0.8	2	0.25	0	-
	0.8	3	0.2	0.338	0.051
	1.4	2	0.98	0	-
500	0.8	3	0.34	0	-
	1.2	2	1.2	0	-
550	-0.6	2	-0.46	0	-
	2.0	2	13.62	0.343	0.0007

Table 2.1: Results for electrochemical ammonia synthesis using a 10mm, AgPd working electrode with a $BaZr_{0.4}Ce_{0.4}Y_{0.1}Yb_{0.1}O_3$ electrolyte, and in 3%H_2O-Ar and dry N_2

Upon increasing the duration of the 0.8V potential past 30 minutes to 2 hours or 3 hours, the rate of ammonia production is, at best, a magnitude smaller. The current density remains consistent throughout these experiments (0.19 ± 0.06 mA/cm^2), however the inconsistency in the rate and efficiency for longer tests suggest that the experiments performed for $\leq$30 minutes are not accurate. Additionally, increasing the temperature from 450° to 500°C nearly doubles the current density, but no discernible amount of ammonia is obtained after 3 hours of operating at 0.8 volts. The increase in the proton conductivity with elevated temperature does account for the higher current density, but this is insufficient for improving the ammonia synthesis rate.

Apart from the aforementioned results, ammonia is only ever obtained at 550°C using 2V; the rate being 0.343x10^{-12} $mol/cm^2 \cdot s$ and an efficiency of 0.0007%. The resulting current density of the electrochemical cell obtained when exposed to both 3%H_2O-Ar and

dry nitrogen (Figure 2.5) is slightly higher than when the cell is exposed to just 3%H_2O-Ar. This is a common indicator shown in the literature to suggest that this higher current density could be due to electrochemical ammonia synthesis. In comparison to a previously published article[82] that used the same potential and operating conditions, the low rates are nearly identical (literature: 0.3x10^{-12} mol/cm^2·s) and the magnitude of the current density (13.62 mA/cm^2) is well above that in the literature (5 mA/cm^2).

Temperature (°C)	**Electrolyte**	**Reactants**	**Rate (mol/cm^2·s)**	**Faradaic Efficiency (%)**	**Reference**
500-600	$BaZr_{0.8}Y_{0.2}O_3$	H_2O-N_2	8.5×10^{-11}	0.33	[83]
500-600	$BaZr_{0.8}Y_{0.2}O_3$	H_2O-N_2	4.9×10^{-11}	0.46	[83]
500-650	$ScCe_{0.95}Yb_{0.05}O_3$	H_2O-N_2	3×10^{-13}	<1	[82]
400	CGO-$(Li/Na/K)_2CO_3$	H_2O-N_2	1.83×10^{-10}	5.4	[84]
400-450	CGO-$(Li/Na/K)_2CO_3$	H_2O-N_2	1.23×10^{-10}	0.55	[85]

Table 2.2: Experimental studies performed with H_2O and N_2

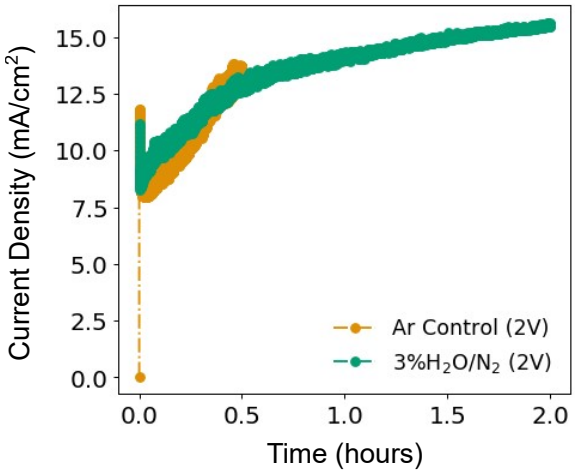

Figure 2.5: Current density for experimental test at 550°C for 2 hours

2.2.2.2 Operating in 3%H_2/N_2

When a mixture of nitrogen and hydrogen gas are both fed into the cathode, then the electrochemical ammonia synthesis process can use both the protons emanating from the anode as well as from hydrogen gas that dissociates on the surface of the working electrode. First, consider the case of electrochemical ammonia synthesis using 3mm diameter working electrode samples tested under the aforementioned gas atmosphere (Table 2.3). Upon applying a 0.8V potential for 30 minutes at 450°C, the electrochemical cell reaches a maximum rate and efficiency of 53.9x10^{-12} mol/s*cm^2 and 8.9% respectively. Although these rates are higher than those tested under the dry nitrogen conditions, additional experiments tested beyond 30 minutes again show a large drop in the rate and efficiency. This is seen when 10mm samples are tested for 2 hours, yielding rates on the order of 10^{-13}. As well, it is expected that the larger 10mm diameter working electrode would yield a higher concentration of ammonia compared to that of the 3mm diameter samples, but this was not the case. Since the rate is normalized to the geometric area of the working electrode, it may just be that the perceived increase in rate for the 3mm samples is simply due to the smaller geometric area (i.e. 3mm: 0.0707cm^2 vs 10mm: 0.785cm^2).

Temp (°C)	**Diameter (mm)**	**Voltage (V)**	**Duration (hours)**	**Current Density (mA/cm^2)**	**Rate (mol/cm^2*s) $*10^{-12}$**	**Faradaic Efficiency (%)**
450	3	0.8	0.5	0.24	53.9	6.5
	3	0.8	0.5	0.13	26.7	5.9
	3	0.8	0.5	0.12	37.3	8.9
	10	0.8	3	0.19	0.34	0.051
	10	-1.2	2	-0.45	0	-
500	10	-1.2	2	-0.5	0.6	0.035

Table 2.3: Results for electrochemical ammonia synthesis using a 3mm or 10mm, AgPd working electrode with a $BaZr_{0.4}Ce_{0.4}Y_{0.1}Yb_{0.1}O_3$ electrolyte, and using $3\%H_2O$-Ar and $3\%H_2/N_2$

The results indicate several key aspects to consider when synthesizing ammonia electrochemically using proton conducting electrolytes under low hydrogen concentrations. Firstly, the duration of these experiments should be well above 30 minutes and should be repeated at consecutively increasing time intervals in order to remove ambiguity as to whether ammonia is being produced. The results presented here did not show an increase in rate or efficiency with increasing test duration, which indicates that the cell is not effective to produce ammonia under these hydrogen deficient conditions. This procedure should also be applied for future studies looking to characterize different electrolytes for ammonia synthesis, given that the vast majority of articles only test their setups for 30 minutes at most. Secondly, the low magnitude of the rates obtained in the two different gas compositions illustrate that the proton concentrations are much too low to use as a means of producing ammonia or to determine the performance of an electrolyte. A plethora of studies in the literature obtained much higher rates on the order of 10^{-9}, but they all used pure hydrogen at the anode instead of steam (i.e. $3\%H_2O$ at atmospheric pressure) and at times incorporated

stoichiometric ratios of hydrogen on the cathode side. Furthermore, these studies similarly used AgPd symmetric cells with electrolytes that had comparable performance to that of $BaZr_{0.4}Ce_{0.4}Y_{0.1}Yb_{0.1}O_3$. Experiments that use steam at the anode must dissociate the water molecules first and subsequently oxidize hydrogen to form protons, whereas experiments that use pure hydrogen need only the oxidation step. Thus, for further studies that seek to determine the efficacy of a proton conducting electrolyte, it would be beneficial to begin with pure hydrogen at the anode to achieve better results.

2.3 Conclusion

In this study, a $BaZr_{0.4}Ce_{0.4}Y_{0.1}Yb_{0.1}O_3$ proton conductor is synthesized, characterized and implemented into an electrochemical setup. It is found that the rate and efficiency of ammonia production using this system is comparable with the results found in literature for similar systems using a solid state proton conductor. However, further experiments suggest that results obtained in this study, and in the literature that use steam as a proton source, are erroneous because the supply of protons to the working electrode is insufficient. It is recommended for future studies to conduct time-dependency tests to confirm that ammonia is continuously synthesized, and to perform these experiments for at least 2 hours. As well, steam is determined to be an insufficient proton source to adequately assess the performance of solid-state proton conductors, and instead pure hydrogen should be implemented at the anode.

CHAPTER 3

Using Na^+ and K^+ Promoters to Electrochemically Promote Ammonia Synthesis

3.1 Background

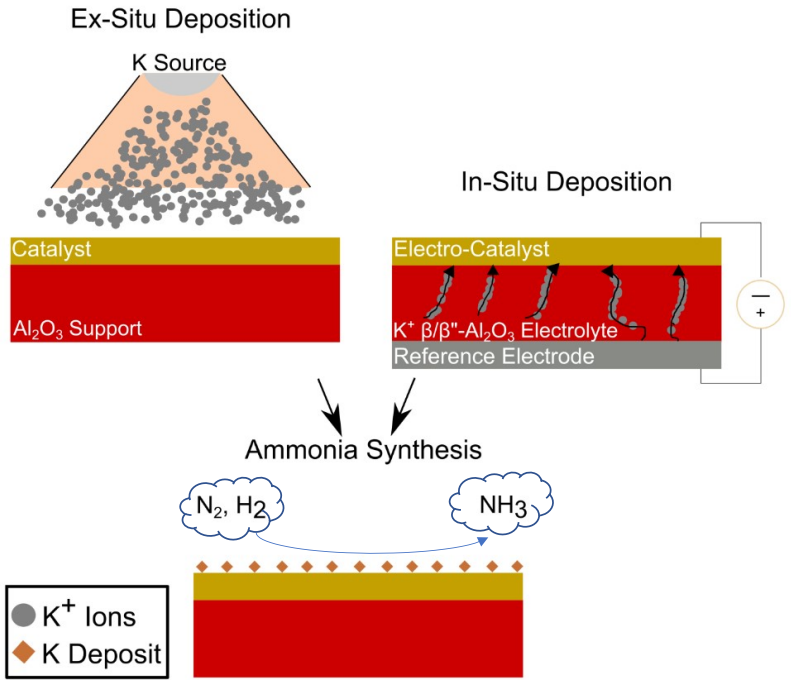

Figure 3.1: Comparison of a traditional ex-situ deposition techniques versus in-situ deposition of promoters (e.g. NEMCA)

High ammonia synthesis rates are commonly obtained in both thermo-catalysis and electro-catalysis via engineering high surface area and high activity catalysts. Doping an iron (magnetite) catalyst with potassium is often implemented to improve the thermo-catalysis of ammonia.[24] Further studies performed on this catalyst in a stoichiometric gas environment of nitrogen and hydrogen concluded that the presence of potassium caused the preferential increase in nitrogen adsorption and suppressed hydrogen adsorption. Since hydrogen covers more of the active sites than nitrogen without a promoter, this change in gas adsorption allows for the reaction pathway to proceed faster.

Sodium is widely used to promote nitrous oxide reduction on platinum and copper cat-

alysts.[86–88] The phenomenon is caused by cations inducing a change in the work-function of the catalyst.[89,90] This in turn causes electropositive molecules to have a weakened adsorption strength (e.g. H_2), while electronegative molecules (e.g. N_2) form a stronger adsorption bond. When an electrochemical setup is used to add the promoters to the catalyst surface, the phenomenon is referred to as 'non-faradaic electrochemical modification of catalytic activity' (NEMCA).[91] The main advantage of using NEMCA promotion as opposed to traditional methods of adding the promoters is that the process can be performed in-situ, which allows for dynamic and reversible control over the chemical synthesis (Figure 3.1).

Potassium is often implemented as a promoter for industrial, catalytic ammonia synthesis; however, there are few electrochemical studies that compare its use to that of other promoters, or test its performance under different system conditions. Such comparisons can further aid our understanding of how different promoters influence the electro-catalytic activity of nitrogen reduction. As well, testing the performance of promoters in a different system condition, such as non-stoichiometric gas environment, can test the limits of the promoters to enhance the catalytic rate. **Herein, the type of promoter and non-traditional gas environment are explored by using electrochemical promotion to compare the performance of sodium and potassium promoters to synthesize ammonia at 450°C and 500°C, and in a nitrogen-rich gas environment (3% H_2/N_2)**.

3.2 Methods

Sodium beta/beta" alumina electrolyte (i.e. Na^+ BASE) is synthesized by calcining stoichiometric amounts of sodium carbonate (Na_2CO_3) and boehmite (Dispal 10F4, Sasol), along with lithium carbonate (Li_2CO_3) to stabilize the structure at 1200°C for 10 hours. Zirconia powder (5wt%) is mixed in with the synthesized Na^+ BASE powder for increased mechanical strength and improved stability in a humidified environment. Samples are then pelletized and sintered at 1600°C for 25 minutes. Additionally, the potassium beta/beta"

alumina electrolyte (i.e. K^+ BASE) samples are synthesized by using the vapour phase exchange method.[11,92,93] This involves pressing Na^+ beta/beta" pellets, covering them in 12wt% $KHCO_3$ in α-Al_2O_3, sealing the contents in a crucible, and calcinating at 1400°C for 6 hours. The vapour phase exchange method is repeated 4 times with replenished potassium carbonate each time to exchange the sodium ions for potassium. The Na^+ and K^+ conducting electrolyte samples are then polished and coated with AgPd on both sides, dried at 60°C, and heat-treated at 600°C for 1 hour. To characterize the electrolyte and catalyst samples, XRD and XRF are implemented.

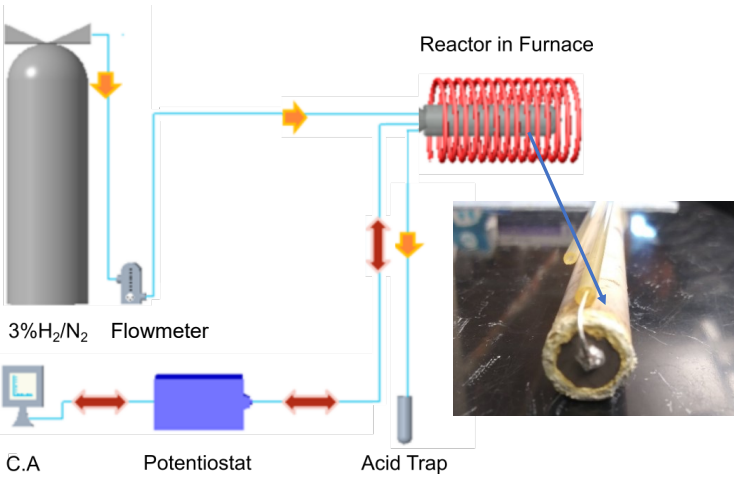

Figure 3.2: Electrochemical promotion process and collection of NH_4^+ sample

3.2.1 Characterization

The crystal structure of the electrolytes are obtained using X-ray diffraction (Rigaku), which implemented a Cu-Kα radiation source operating at 40kV and 40mA. The resulting spectra are measured at a rate of 20° per minute for 2θ values within 10 and 80 degrees. As well, a portable X-ray fluorescence spectrometer (Niton XL3t GOLDD+) is used to obtain the elemental composition of the electrolyte samples.

Rate and efficiency measurements are also conducted in 3%H_2/N_2 gas at 450°C and 500°C for 2 hours at 0.67V (Figure 3.2). Prior to applying a potential, a surface cleaning procedure is implemented using 1.2V. This serves to rid the catalyst surface of promoters

that migrated to the surface due to thermal migration. The effluent gasses emanating from the reaction chamber are captured in a 10 mL acid trap (0.001M H_2SO_4) and partake in the Berthelot reaction to form indophenol. The concentration of ammonia is ascertained by using a UV-VIS spectrophotometer and measuring the absorbance of the indophenol at 655 nm. Control experiments are performed at open circuit voltage (O.C.V) to account for background ammonia residing in the gas stream or in the reactor itself. The reported rate and efficiency values are found using the equations below.

$$Rate = \frac{[M_V] - [M_{OCV}]}{A * t} * V \tag{3.1}$$

$$Efficiency = \frac{3 * Rate * F}{J} * 100 \tag{3.2}$$

where, [M_V]: concentration (mol/L) of NH_3 due to 0.67V bias for 2 hours; [M_{OCV}]: concentration (mol/L) of NH_3 obtained at the open circuit potential for 30 minutes; A: catalyst geometric area (cm^2); t: test duration (s); V: volume of acid trap (mL); F: Faraday's constant (C/mol); J: current density (A/cm^2);

3.3 Results & Discussion

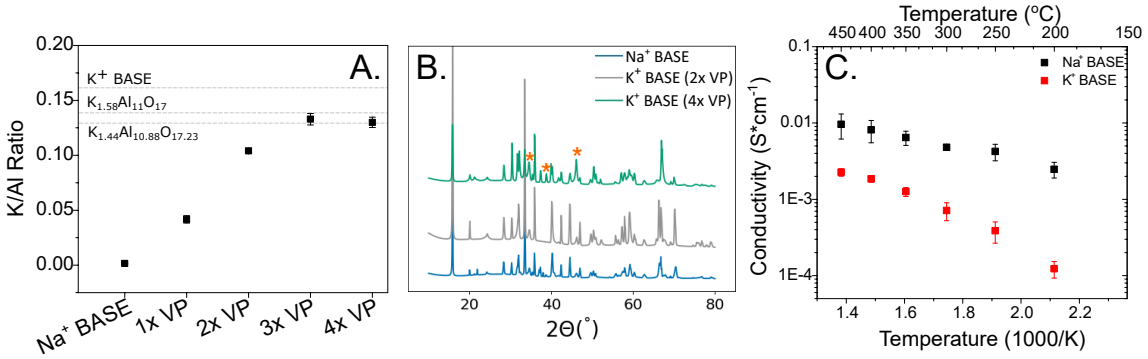

Figure 3.3: (A.) K/Al ratio for pristine Na^+ BASE and corresponding samples that underwent vapor phase (VP) ion conversion 1-4 times, (B.) XRD spectra of the as synthesized Na^+ BASE and K^+ BASE samples that underwent vapor phase synthesis twice and four times respectively, (C.) Ionic conductivity of Na^+ and K^+ BASE within 200°C and 450°C; *Peaks corresponding to K^+ BASE (JCPDS 21-618)[11], $K_{1.58}Al_{11}O_{17}$ (ICSD 201177)[12] and $K_{1.44}Al_{10.88}O_{17.23}$ (No. 84-0819)[13]

The Na^+ and K^+ beta/beta"-alumina electrolytes are characterized in Figure 3.3. For the synthesis of K^+ BASE, XRF analysis (Figure 3.3A) indicates that potassium is increasingly incorporated into the initial sodium beta"/beta-Al_2O_3 structure throughout the four rounds of vapour-phase exchange. The process is highly reproducible, as noted by the low variability, so these samples were used for the electrochemical promotion of ammonia. It should be noted that the final K/Al ratio for the samples is 0.13, which is slightly lower than that of pure β"-Al_2O_3 (K/Al=0.16). This could be due to sodium loss during the ion exchange process that prohibits additional potassium from entering into the spinel structure. To that effect, the K/Al ratio suggests that a potassium-aluminate structure is obtained instead. However, XRD spectra illustrates peaks distinct to beta and beta" alumina.

The main characteristic peaks for beta-alumina are 33.3° and 44.5°, and for beta"-alumina the characteristic peak is found at 46.0°[94]. The apparent fraction of β"-Al_2O_3 to β-Al_2O_3 is 84% for the Na^+ BASE samples and 59% for the K^+ BASE samples, as obtained using the equation below:

$$f(\beta") = 1 - I(\beta)/(I(\beta) + 0.851I(\beta")) \tag{3.3}$$

where I(β") is the intensity obtained from XRD (Figure 3.3B) at 46.0° and *I(β)* is the intensity obtained at 44.5°. The two fractions are lower than the commercially obtained fraction of β"-Al_2O_3 (100% for Na^+ BASE and between 85-90% for K^+ BASE (Ionotec Ltd.)), which coincides with the lower K/Al ratio. Consequently, this results in a slightly lower ionic conductivity for K^+ BASE, and an ionic conductivity consistent with the literature for Na^+ BASE (Figure 3.3C). In essence, the performance of these electrolytes are more than sufficient for an electrochemical promotion study, since the electrochemical cells need to be able to sustain current on the order of microamps. When the Ag-Pd symmetric cells operate at 450°C and 500°C, this requirement is fulfilled by applying the 1.2V surface-cleaning potential, which rids the surface of promoters (Na or K) and consequently reduces the current from milliamps to microamps prior to the electrochemical synthesis of

ammonia.

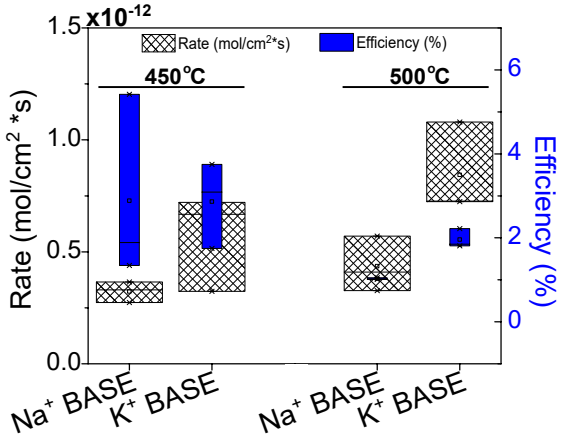

Figure 3.4: Rate and efficiency for electrochemical ammonia promotion using AgPd —X^+BASE—AgPd samples (X: Na or K) tested using 0.67V and 3%H_2/N_2 gas, at 450°C and 500°C respectively for 2 hours

Upon performing the electrochemical promotion, it is observed that ammonia is effectively synthesized using the low hydrogen concentration of 3% balanced with nitrogen (Figure 3.4). Potassium promoted samples achieved a maximum rate and efficiency of 0.84x10^{-12} mol/cm^2*s and 2.86%, and for sodium a maximum rate of 0.57x10^{-12} mol/cm^2*s and efficiency of 2.88%. Going from 450°C and 500°C, the NH_3 synthesis rate increased 1.48x times for the K^+ promoted samples, and the Na^+ promoted samples increased 1.35x. As well, the K^+ samples are revealed to have a higher rate than the Na^+ samples at both 450°C and 500°C, equivalent to a factor of 1.77x and 1.94x respectively. These results correlate with the selection of traditional Haber catalysts, since potassium is often chosen as the promoter of interest instead of sodium. For traditional catalysts, it is accepted that the size of the alkali metal affects the synthesis rate by inducing a stronger dipole moment, which could account for potassium having the higher rate. This also affects the atoms' electronegativity, in which case sodium has a higher electronegativity than potassium. Thus, potassium can be more willing to give up its lone electron and donate it to the catalyst for a more effective decrease in the work-function.

Apart from the results presented here, only one other study to date delves into using an

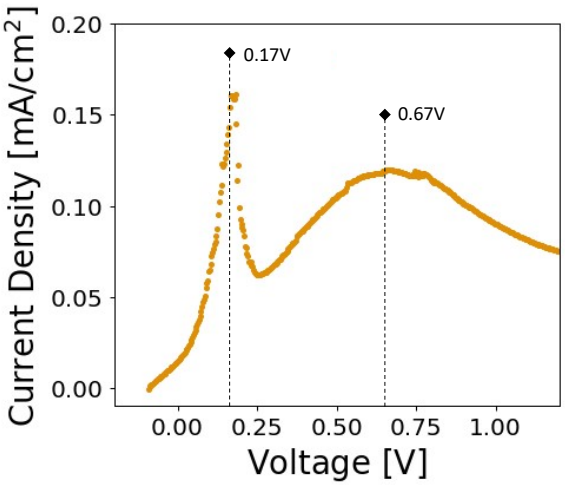

Figure 3.5: Linear sweep voltammogram of a representative AgPd—Na^+ BASE—AgPd electrochemical cell obtained in 3%H_2/N_2 gas; A second peak at 0.67V only appears in the 3%H_2/N_2 gas and not in an inert environment

alkali-metal, electrochemical promotion approach for ammonia synthesis.[95] With the use of a potassium-ion conducting electrochemical cell operating at atmospheric pressure, the authors identified the optimal rate of ammonia synthesis conditions to be at 500°C, using a 1:1 partial pressure of nitrogen to hydrogen, and at a voltage near 1V. The optimal voltage of 1V is then correlated to the anodic peak they found at 1V using cyclic voltammetry. This observation justifies our own selection for operating at 0.67V, since it is based on observing a 0.67V peak that only appears in the 3%N_2/H_2 environment and not in an inert environment (Figure 3.5 and A.1).

It is important to note that the ammonia formation rates are quite low in all of the presented results, and this is primarily due to the low hydrogen concentration. When a typical stoichiometric gas environment is used, hydrogen occupies most of the active sites on palladium or bimetallic metal surfaces (i.e. AgPd).[96] Thus, using a gas environment with nitrogen gas as the majority component allows for more nitrogen to be adsorbed onto the catalyst than with a stoichiometric gas mixture. Furthermore, adding alkali promoters to this catalyst further increases the number of dinitrogen molecules on the catalyst, which in turn decreases the occupancy of atomic hydrogen. Since ammonia is produced, it is

clear that the promoters can still optimize the coverage of hydrogen under these conditions, albeit to a weaker extent than if a much higher hydrogen partial pressure is implemented.

3.4 Conclusion

Electrochemical technologies are important decentralized systems that can aid in decarbonization of energy and chemical industries.[97,98] Herein, potassium promoters are examined for intermediate temperature ammonia production.[24] Slightly higher formation rates and efficiencies were observed for potassium promoted samples than sodium promoted samples under sub-stoichiometric conditions. This finding coincides with general trends of alkali metal promoters used in catalysis, and justifies the use of potassium in commercial Haber catalysts. This study illustrates that electrochemical promotion is a useful technique for comparing promoters in situ, while closely maintaining the same experimental conditions (i.e. maintaining the same beta"-structure for ion mobility).

Acknowledgment

The authors were supported by the National Science Foundation under grant No. 1847029 and 1821573. The authors would like to thank Dr.Goodbred for his assistance in acquiring the elemental analysis using the portable x-ray fluorescence analyzer.

CHAPTER 4

Simultaneous Cu^{2+} Reduction and Ammonia Synthesis using Ascorbic Acid Treated VO_2 & RGO Catalyst

4.1 Background

To improve the electrochemical synthesis of ammonia, efficient catalysts need to be implemented. The nitrogen reduction reaction is particularly difficult to perform because of the strong triple bond of molecular nitrogen.[99] Currently, there are only a handful of complex systems that can dissociate molecular nitrogen under ambient conditions to synthesize ammonia at a reasonable rate. For example, there is a high performance system that uses a "lithium-mediated reaction" approach which requires the use of lithium metal to form lithium nitride.[100,101] This type of system needs to be sealed to prevent lithium from reacting with air or moisture, which are nontrivial tasks. For other systems, the rate can be increased by activating the dinitrogen molecule as it is adsorbed; this in-turn can lower the activation energy of the potential determining step (PDS). The dinitrogen molecule can be "activated" through back-donation of electrons from the catalyst. This decreases the bond length, thus reducing the energy required for the sequential protonation steps.[102] Thus, additional research should focus on identifying catalysts that can activate molecular nitrogen.

The presence of vanadium in biological nitrogen reduction motivates the study of vanadium-based catalysts for electrochemical ammonia synthesis. Nitrogenase enzymes are responsible for biological NRR in plants and bacteria, to which there are only three types: Mo-nitrogenase, V-nitrogenase, and Fe-nitrogenase. Molybdenum nitrogenase (Mo-nitrogenase) refers to the Fe-Mo cofactor that is the active center, while V-nitrogenase has an Fe-V active center, and Fe-nitrogenase has only an iron center. Although Mo-nitrogenase attains a higher rate and efficiency than the others, it is clear that vanadium aids in the synthesis of ammonia, given that without it (i.e. Fe-nitrogenase) the rate and efficiency decrease. The

catalytic ability of these elements has informed the design of new electrocatalysts for ammonia synthesis, such as transition metal nitrides. Vanadium nitride is identified as one of the most active and stable nitrides at its 100 facet, more so than both FeN and MoN.[103,104] These nitride catalysts are thought to follow the Mars van Krevelen mechanism, which can decrease the energy needed to adsorb nitrogen gas due to nitrogen vacancies in the catalyst. As well, vanadium oxide particles are the latest class of vanadium-based catalysts to be tested for ammonia synthesis.[18,105–107] Implementing non-noble metal catalysts like vanadium oxides that are also abundant can help to reduce cost if they can reliably synthesize ammonia at high rates.

Attempts to implement monoclinic VO_2 as a catalyst in ambient conditions yielded negligible amounts of ammonia (Appendix A.3). Several vanadium oxide catalysts studied in literature (e.g. V_2O_3) are electrically conductive at room temperature and perform moderately well in synthesizing ammonia. That is why this study treats VO_2 (M) particles with ascorbic acid (AA) to reach a more conductive phase, and also incorporates reduced graphene oxide (RGO) to further improve the electrode conductivity. During the process of preparing the electrode, copper ions are unexpectedly incorporated onto the electrode, which are also reduced during electrocatalysis. **Thus, this project delves into the performance of this complex electrode, and two hypotheses are challenged to account for the ammonia synthesis process on the electrode.**

4.1.1 Rutile Phase VO_2

As a semiconductor, VO_2 (M) can transition from an insulating phase to a metallic phase. By increasing the temperature of the particles past the metal to insulator transition temperature (MIT), the metallic rutile phase can be achieved.[108] Although this is a facile method of reaching the rutile phase in principle, it limits the ability to perform electrocatalysis at lower temperatures. Doping the VO_2 structure with high valency metals (e.g. tungsten or molybdenum) can effectively lower the transition temperature so that the rutile structure is

attained at room temperature.[109,110] This is a valid option that is worth exploring, however further optimization of the synthesis method is required to implement the dopant. There are other methods of attaining the rutile phase, but the one deemed suitable for this study is to incorporate protons into the VO_2 structure.

4.1.1.1 Dosing VO_2 (M) with Protons

Dosing monoclinic VO_2 with protons is another method used to attain the conductive rutile phase. Acidification of VO_2 leads to the formation of V^{4+} ions instead of proton incorporation, so other methods were developed to protonate VO_2 (M). Traditional techniques are rather involved and costly, spanning from electrochemical insertion[111] to catalytic spillover[112]. Electrochemical insertion of protons into VO_2 (M) is performed using a non-aqueous electrolyte at an applied current. This led to a relatively small percentage of proton insertion (i.e. for H_xVO_2, $0.02 \leq x \leq 0.04$). In the case of catalytic spillover, this procedure uses a catalyst powder like palladium mixed in with VO_2 (M). The mixed powder is heated to around 200°C in the presence of hydrogen, so that palladium adsorbs hydrogen and then hydrogen can spillover to the VO_2.

Simpler methods of incorporating protons into the monoclinic VO_2 structure involve immersing VO_2, typically as a film, into a solution that won't fully reduce it to V^{4+} ions. One such concept[113] used an acidic acid solution (2wt% H_2SO_4) and a metal particle (1 mm) resting on the VO_2 film. Depending on the metal, its low work-function led to co-doping of electrons and protons into VO_2 to form the rutile phase. Copper has a work-function that leads to rutile $H_{0.25}VO_2$, while aluminum and zinc have an even lower work-function that leads to a heavily protonated, insulating phase of VO_2. Another method uses ascorbic acid to protonate VO_2[114], which also functions by co-doping electrons and protons into the VO_2 structure. Essentially, an ascorbic acid molecule chelates onto a VO_2 particle surface, wherein electrons are donated. This drives protons from the acidic environment into VO_2, thereby expanding the crystal lattice to form its rutile phase. Most recently,

an experimental design implemented $NaBH_4$ to protonate VO_2, in which $NaBH_4$ powder covers a VO_2 film in a beaker, followed by immersion in DI water[115]. This simple process leads to rutile VO_2, with the option of obtaining "heavily protonated" VO_2 by heating the beaker to 80 °C.

In terms of implementing protonated, rutile H_xVO_2 as a catalyst on carbon paper electrodes, it is worth examining whether these three simple techniques can be used. Since an ink of the catalyst needs to be prepared, the VO_2 (M) catalyst particles need to be protonated beforehand. The copper-acid co-doping method is efficient for connected films, but does not seem feasible for protonating a batch of VO_2 powder. The ascorbic acid method is capable of synthesizing H_xVO_2, but with residual ascorbic acid remaining on the particles. Finally, the $NaBH_4$ technique appears to be the best method because the particles can be protonated rapidly without residual molecules. At the time of this study however, the $NaBH_4$ technique had not yet been published, and so we resolved to use the ascorbic acid method along with a series of cleaning steps to obtain H_xVO_2.

4.1.2 Implementing Reduced Graphene Oxide (RGO) for Ammonia Synthesis

Reduced graphene oxide (RGO) is implemented in many electrochemical systems including batteries[116–118], capacitors[119–121], and for electrocatalysis[122–124]. Prior to 2018, RGO was not investigated as a component for the NRR reaction, but in the last few years it has been incorporated with a number of other active materials (Figure 4.1). In these studies it is observed that RGO is not active for this reaction; with exception to it being modified with tannic acid or chlorine[16,125]; however, RGO does play a beneficial role in the synthesis of ammonia. Among several ideal characteristics, RGO can improve the dispersion of nanoparticles[126,127], the electrical conductivity of the electrode[128,129], and the adsorption kinetics of hydrogen[18,130].

One study showed that copper and palladium on RGO respectively achieved improved synthesis of ammonia when compared to the absence of RGO.[131] The high surface area of

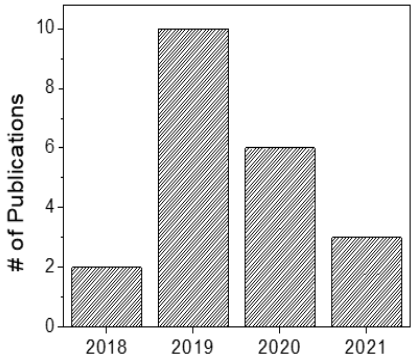

Figure 4.1: Instances of using RGO for electrochemical ammonia synthesis; Compiled from Web of Science

RGO is said to maximize the exposure of the metal active sites, thereby leading to improved N_2 adsorption capacity. As well, RGO is said to reduce the electron transport barrier due to it maintaining a continuous electron pathway. Another study implemented yolk-shell-structured $Fe@Fe_3O_4$ sandwiched between RGO and carbon paper[132]. The authors note that RGO and the nanoparticles display a synergistic effect by implementing good electrical contact, preventing oxidation of the metal particles, and suppresion of the hydrogen evolution reaction. Lastly, another study focusing on TiO_2 with RGO mentions that its decent performance is due to having good dispersion of the nanopartiles and fast NRR kinetics due to RGO. From theses experimental studies, it is clear that RGO can enhance the electrochemical synthesis of ammonia which is why it was chosen as a component in our catalyst ink formulation.

4.2 Methods

4.2.1 VO_2 Synthesis

Vanadium dioxide particles are produced using a hydrothermal synthesis route (previously optimized by Dr.Aaron Daniel) using V_2O_5 as the vanadium precursor (Fig 4.2). The synthesis is performed at 90°C in a three-neck, round bottom flask into which the V_2O_5 precursor is introduced along with 10mL of DI water. As the solution is rigorously stirred,

it is first acidified with concentrated sulfuric acid (H_2SO_4), reduced using hydrazine monohydrate (N_2H_4-H_2O), and finally precipitated out to form $V(OH)_2NH_2$ upon adding sodium hydroxide to reach a pH of 4. The volume of sulfuric acid, hydrazine monohydrate, and

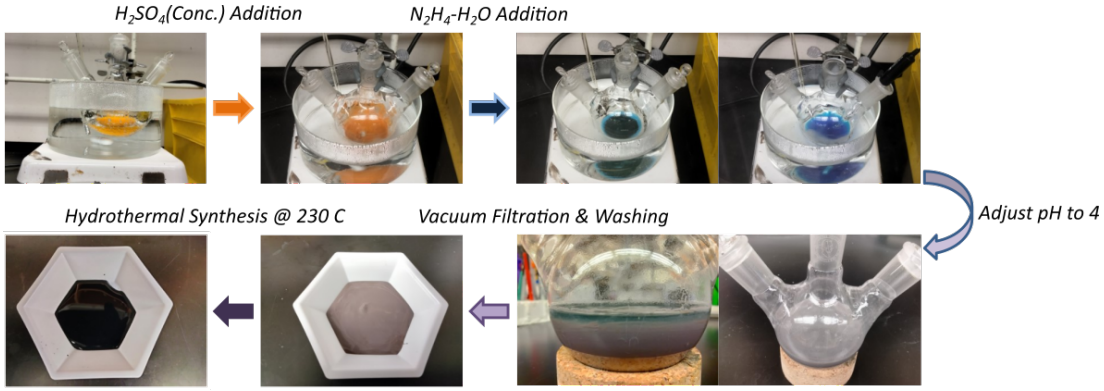

Figure 4.2: Hydrothermal synthesis of vanadium oxides

sodium hydroxide are scaled based on the precursor mass. The precipitate is then vacuum filtered and washed with DI water. Subsequently, the precipitate is added to a Teflon cup with 25 milliliters of DI water and stirred for 1 hour. The Teflon cup is then sealed in a steel container and placed into an oven to allow the hydrothermal reaction to take place at 230°C for 48 hours. Afterward, the solution in the Teflon cup is disposed, leaving solely a pellet of pure VO_2. The pellet is then sequentially washed in water (3x) and ethanol (3x) by placing in in a centrifuge for at least one minute per wash cycle. Finally, the VO_2 catalyst is dried in an oven at 100°C overnight, crushed using a mortar and pestle, and stored in glass vials.

The VO_2 (M) powder is treated with ascorbic acid in order to incorporate protons within its structure. This is done by adding 10mg of monoclinic VO_2 to 1mL of ascorbic acid (i.e. AA). The ink is then vortexed and subsequently sonicated for 1 hour. Then, the ink is washed by centrifuging the treated VO_2 with DI water and 0.05M H_2SO_4 four times each.

4.2.2 RGO Synthesis

Using ascorbic acid as the reducing agent[133,134], reduced graphene oxide (RGO) is synthesized from commercial graphene oxide (GO) (Graphene Supermarket) solution. Two

milliliters of the graphene oxide is heated and mixed at 80°C with 0.277M ascorbic acid for 1 hour. Afterward, the precipitate is washed using 1M HCl and DI water repeatedly, ending with the DI wash step. The precipitate is then vacuum dried for 1.5 hours. Raman spectroscopy is used to characterize the formed precipitate.

4.2.3 Electrode Preparation

The VO_2 (AA) & RGO catalyst ink is prepared by mixing 1mL of 0.05M H_2SO_4, 30 μL of Nafion, and 10 mg of catalyst (9mg of VO_2 and 1mg of RGO). The inks for the control electrodes, RGO; VO_2 & RGO; VO_2 (AA), and VO_2 (AA) & 3wt% Fe, only differ in terms of the mass of the catalyst (Table 4.1) They are then sonicated for 1 hour and drop cast (40μL) onto a 1.13cm^2, flame-treated MGL190 carbon paper electrode. The electrode is first vacuum-dried, and then it undergoes a pre-electrolysis step (-0.844V vs Ag/AgCl) in 0.05M H_2SO_4 prior to electrochemical experiments. The pre-electrolysis step is implemented as a means of potentially removing lingering ascorbic acid that is still cleaved to the VO_2 particles after the washing steps (discussed further in Appendix A.2; Figure A.2) Finally, all of these electrodes undergo acid treatment by submerging them in 0.5M H_2SO_4 for 48 hours prior to electrocatalysis.

Catalyst	Type	Mass
VO_2 (AA) & RGO	Main Catalyst	9mg VO_2 (AA) & 1mg RGO
VO_2 (AA) & 3wt% Fe	Control	10mg total
VO_2 (AA)	Control	9mg total
VO_2 & RGO	Control	9mg VO_2 & 1mg RGO
RGO	Control	1mg total

Table 4.1: Breakdown of catalyst mass used to prepare the different catalyst inks

Additional control samples consist of electro-deposited copper on MGL 190 carbon paper. These samples are electro-deposited at a potential of -0.2V vs Ag/AgCl in a solution

of $Cu(ClO_4)_2$-$6H_2O$ until the charge passed was equivalent to 2 coulombs. These samples are used for electrocatalysis, and separate group of samples also undergo acid treatment prior to electrocatalysis to be able to directly compare to the other control catalysts from Table 4.1.

4.2.4 Characterization

The catalysts are characterized using x-ray diffraction (XRD) using a Cu K-α source and acquiring spectra within a 2θ range of 10 – 80 degrees. Scanning electron microscopy (SEM) equipped with energy dispersive spectroscopy (EDS) is then used to evaluate the morphology and elemental concentration for each catalyst.

Electrochemical measurements for catalyst characterization are performed in a beaker cell using cyclic voltammetry (CV) and linear sweep voltammetry (LSV) on a CHI 660 potentiostat/galvanostat. These electrochemical methods are performed in 9mL of 0.5M $LiClO_4$ electrolyte using a platinum mesh as the counter electrode, Ag/AgCl reference electrode, and the drop-casted catalyst on carbon paper as the working electrode. Cyclic voltammetry is performed in a beaker cell to identify the redox events associated with the different types of electrodes and gasses in the system. All of the electrodes are prepared using nickel chromium leads (NiCr) instead of copper to control the amount of copper in the system. Beginning with a negative scan from 0V vs Ag/AgCl, 5 full cycles are obtained at a scan rate of 20mV/s between -1.571V and 1.571V vs Ag/AgCl. For each electrode, the cyclic voltammetry technique is first run with argon gas bubbling into the 9mL of 0.5M $LiClO_4$ electrolyte. Afterward, cyclic voltammetry experiments are run with 0.0177g of $Cu(ClO_4)_2$-$6H_2O$ added to the electrolyte, while still under Ar flow. The last set of C.V. experiments are performed in nitrogen (N_2), and run with the same solution made from $Cu(ClO_4)_2$-$6H_2O$ and 0.5M $LiClO_4$. The linear sweep voltammetry experiments are performed on electrodes that previously underwent NH_3 synthesis. The voltage is swept to increasingly positive potentials, in the voltage window of 0 to 1.2V vs Ag/AgCl for a total

of 4 scans.

Nitrogen reduction reaction (NRR) experiments are conducted in an H-cell at a voltage of 0.1V vs RHE (-0.571V vs Ag/AgCl) for 2 hours with nitrogen flow (20 sccm). Control experiments included 2 hour long tests in argon at 0.1V vs RHE, as well as 30 minute long tests at open circuit potential (OCV) just prior to the NRR experiment. For each measurement, 2mL aliquots of the electrolyte are taken out and used in the Berthelot reaction to evaluate the concentration of ammonia. Two milliliters of fresh electrolyte are then replaced to maintain the total volume. Using the calibration curve for ammonia in a 0.5M $LiClO_4$ electrolyte (Figure A.4), the mass of ammonia produced and the faradaic efficiency are evaluated using equations 4.1 and 4.2.

$$NH_3(\mu g) = M_{mol} * V * 17 \tag{4.1}$$

$$\eta_{NH_3}(\%) = 100 * \frac{M_{mol} * V * 3 * F}{17 * C} \tag{4.2}$$

Where $\mathbf{M}_{mol}$: molar concentration of ammonia produced (mol/L); **V**: volume of electrolyte (L); **F**: faraday's constant; **C**: charge passed during NRR (coulombs)

4.3 Results

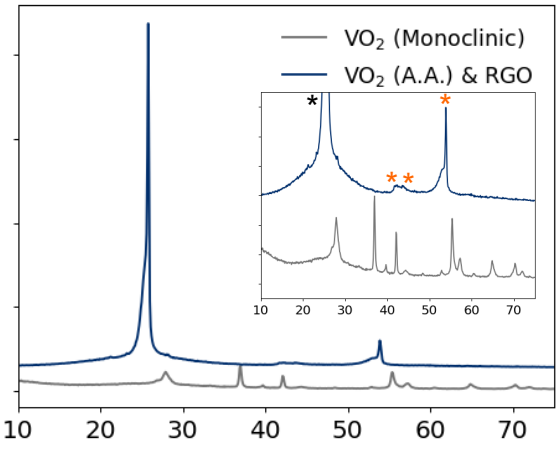

Figure 4.3: XRD of the precursor VO_2 (M) catalyst, and the VO_2 (AA) & RGO catalyst; $\star$ signifies VO_2 (R) phase, while $\star$ corresponds to the VO_2 (A) phase

The VO_2 (AA) & RGO catalyst has x-ray diffraction peaks consistent with a mixed phase of tetragonal VO_2 (A) and VO_2 (R) (Figure 4.3). The previous study[110] that treated VO_2 (M) with ascorbic acid attained a pure phase of rutile VO_2, but the ascorbic acid was not removed from the particles. So the removal of ascorbic acid from the VO_2 (AA) & RGO catalyst during the cleaning steps could account for the resulting mixed-phase. The morphology of the VO_2 (AA) & RGO catalyst also changes from an asterisk shape to an ellipsoid (Figure 4.5). This correlates well with the previous work by Dr.Aaron Daniel, in which the morphology and phase of the VO_2 catalyst changed from monoclinic asterisks to VO_2 (A) ellipsoids as the precursor concentration of V_2O_5 increased.

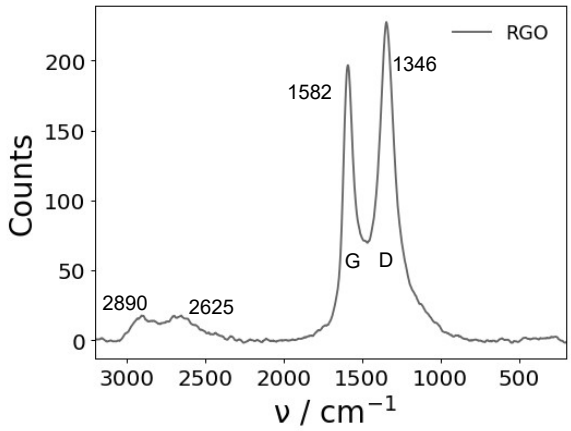

Figure 4.4: Raman spectra of the synthesized reduced graphene oxide (RGO)

Raman analysis of the prepared RGO powder (Figure 4.4) indicates characteristic peaks. Specifically the G-band peak at 1582 cm^{-1} corresponds to sp-2 carbon and the D-band peak at 1346 cm^{-1} which corresponds to disordered carbon. Additionally, the intensity ratio of the D band to the G band is 1.11, which is higher than typical graphene oxide (e.g. I_D/I_G=0.95[20]). The electrical conductivity of RGO is correlated to this ratio, and a value of 1.11 falls within the range of values from literature (i.e. 1.03 to 1.16).[129]

As will be discussed, during the process of electrochemically synthesizing ammonia, copper is simultaneously deposited onto the carbon fibers of the electrode. XRF analysis (Table 4.2) on the electrodes prior to ammonia synthesis reveals that copper resides on the

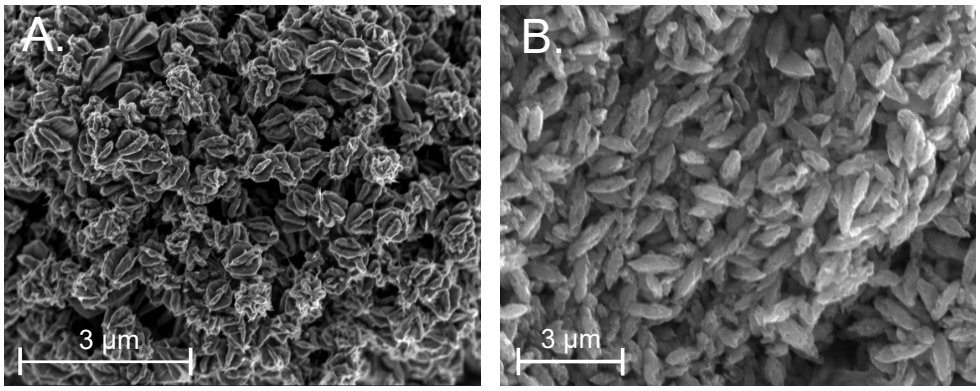

Figure 4.5: SEM images showing the (A.) Asterisk morphology of VO_2 (M) and (B.) Ellipsoid morphology of VO_2 (AA) & RGO

	RGO (ppm)	VO_2 & RGO (ppm)	VO_2 (AA) (ppm)	VO_2 (AA) & RGO (ppm)
As Prepared	$\leq LOD$	$\leq LOD$	$\leq LOD$	$\leq LOD$
Acid Treated	351.24 $\pm$33.99	42.53 $\pm$25.9	40.53 $\pm$25.33	38.8 $\pm$24.23

Table 4.2: XRF concentration of copper on electrodes with the accompanying device error

electrodes due to the acid treatment. The acid treatment causes copper to leach from the copper leads and enter into the solution.

VO_2 (AA) and RGO synthesized the most amount of ammonia compared to all of the control samples that were also tested (Figure 4.6), reaching a maximum of 1.92μg NH_3. Most of the control electrodes reach a value near 0.5μg NH_3 or lower. The only other catalyst that had a similar performance to that of VO_2 (AA) and RGO was VO_2 (AA) with 3wt% Fe, which will be discussed in more detail later. To best understand the trends, the results are reported in terms of total ammonia produced (μg) instead of a rate (μg_{NH_3}/mg_{cat}*hr). This is mainly because the mass of the catalysts are not the same, but are specifically chosen based on their weight percentage in VO_2 (AA) & RGO (i.e. 90% VO_2 (AA) and 10% RGO). This reveals how each component contributes to the ammonia yield.

Delving into the electro-deposited copper controls (Figure 4.6B), the results indicate that 0.2μmol of copper (equivalent to 2 coulombs) deposited on carbon fiber does not ap-

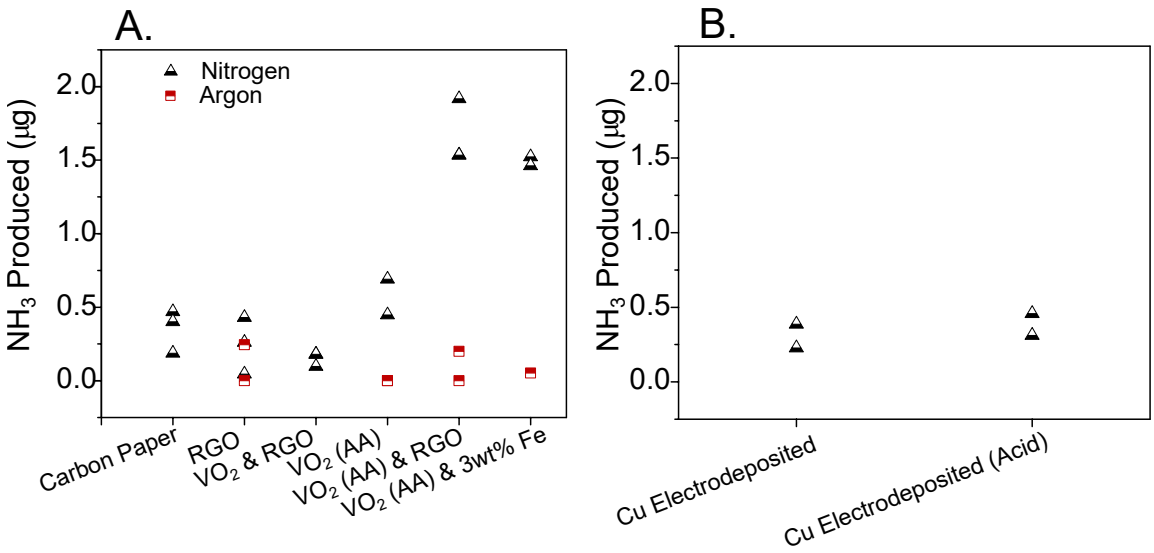

Figure 4.6: A. NH_3 produced (μg) electrochemically in N_2 and Argon respectively at -0.571V vs Ag/AgCl (0.1V vs RHE) for 2 hours; B. Additional control experiments performed in N_2 using copper-deposited electrodes with or without acid treatment

pear to synthesize that much ammonia. Similarly, oxidizing the deposited copper with acid results in a similar low yield. The results suggest that VO_2 (AA) and RGO is catalytically active for ammonia synthesis and that the copper that leached onto the electrode is not, but additional experiments (not shown here) using VO_2 (AA) and RGO without any copper showed zero ammonia production. These results led to two hypotheses to explain the synthesis of ammonia. Hypothesis 1: the copper particles serve as the active site for dinitrogen adsorption, to which nitride ions can migrate and reside on oxygen vacancies of VO_2 (AA) and become protonated to form NH_3. Hypothesis 2: VO_2 (AA) and RGO catalyst facilitates the reduction of Cu^{2+} species in the alkaline electrolyte to form metallic copper particles, which are primarily responsible for the improved synthesis of ammonia. These two theories will be discussed and challenged in relation to the data obtained.

The performance of several catalysts previously studied are presented in Figure 4.8, along with the results obtained in this study for the VO_2 (AA) and RGO catalyst (black star) and the RGO catalyst by itself (red star). One of the trends seen in this plot is the improved performance of catalysts with the addition of reduced graphene oxide, which also

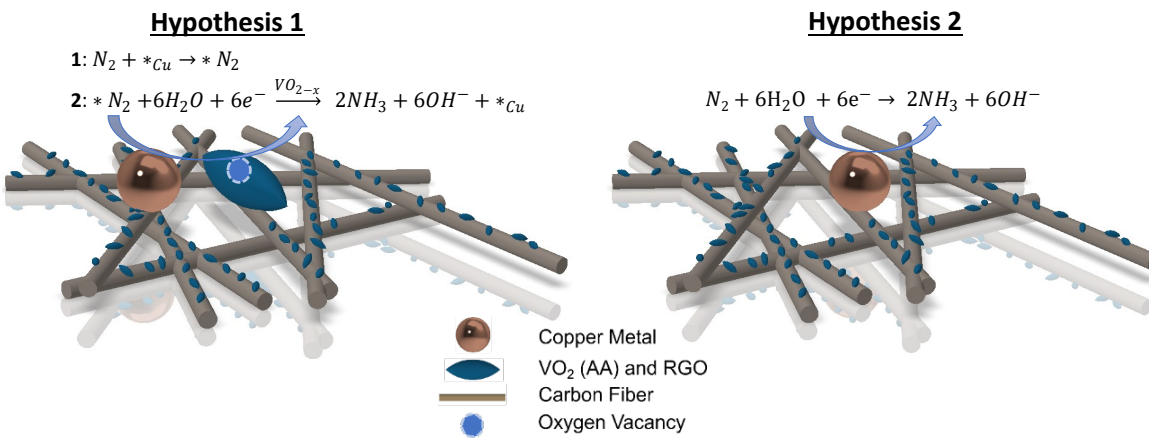

Figure 4.7: Two hypotheses to explain the origin of ammonia synthesis: Hypothesis 1 depicts copper adsorbing dinitrogen molecules and supplying it to the oxygen vacancy sites of VO_2 (AA) & RGO catalyst where ammonia takes place; Hypothesis 2 depicts copper metal as the active catalyst for ammonia synthesis, made possible by VO_2 (AA) & RGO reducing copper ions to copper metal

.

coincides with our results (Figure 4.6A). RGO catalysts alone, however, generally perform poorly and are not considered to have active sites to synthesize ammonia. The common trait of RGO in all of these studies is its ability to improve electron flow between the catalyst particles and the carbon fiber electrode. This may explain why the VO_2 (AA) and 3wt% Fe samples produce a similar amount of ammonia to the RGO counterpart, in that the iron particles were able to reduce the charge transfer resistance of the electrode. Iron itself can be catalytically active towards the NRR reaction in an aqueous H-cell system[19,135], but at the applied potential of 0.1V vs RHE (-0.571V vs Ag/AgCl) it is unlikely that it can aid in the synthesis directly. Comparing the potentials used in the literature to the VO_2 (AA) & RGO catalst (Figure 4.8), the study using electro-deposited copper (Cu-2) at 0V vs RHE is closest to the applied potential and synthesizes a similar amount of ammonia. The 0.1V potential is quite positive even when compared to other vanadium oxide-based catalysts. Table 4.3 clearly shows that the optimal potential for the vanadium oxide electrolytes in neutral media (0.1M Na_2SO_4) is between -0.5 and -0.7V vs RHE. With regards to the two hypotheses mentioned previously, the results suggest that the active sites for nitrogen

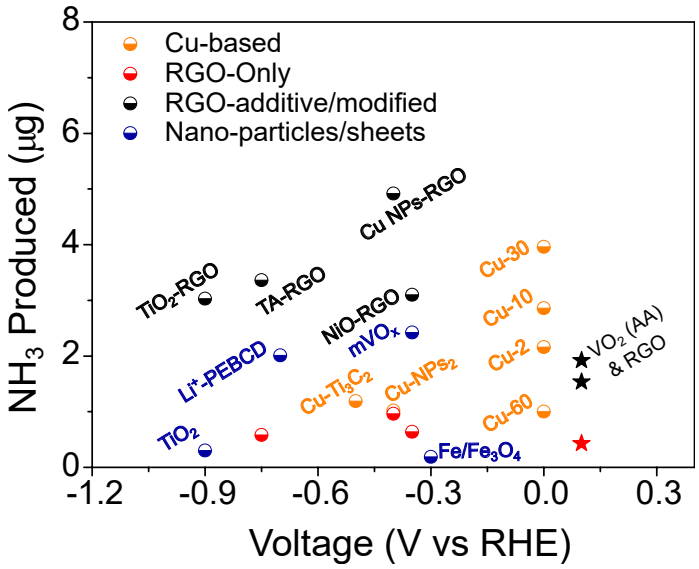

Figure 4.8: NH_3 produced (μg) after 2 hours* electrochemically using VO_2 (AA) and RGO in this study compared with literature; Catalysts: TiO_2-RGO[14], Li^+-PEBCD[15], TA-RGO[16], Cu-Ti_3C_2[17], mVOx[18], NiO-RGO[18], Fe/Fe_3O_4[19], Cu NPs-RGO[20], Cu-2 to Cu-60[21]; *Only the Fe/Fe_3O_4 catalyst underwent electrolysis for less than 2 hours

Catalyst	Potential (V vs RHE)	NH_3 Produced (μg_{NH_3})	Reference
mVO_x-RGO	-0.35	37.68	[18]
VO_2-Hollow Microspheres	-0.7	5.94	[105]
V_2O_3-Nanorings	-0.6	1.89	[106]
V_2O_3-MOF	-0.6	4.92	[107]
V_3O_7-H_2O Monolith	-0.55	3.63	[136]

Table 4.3: Vanadium oxide catalysts performance in literature

reduction are due to copper and not the vanadium oxide.

Further interpretation of the performance of the VO_2 (AA) and RGO electrode involves time and voltage-dependency experiments. The time-dependency experiment (Figure 4.9) shows that the amount of ammonia produced is high within the first hour, however with additional time/charge passed the amount of ammonia appears to stagnate. Likewise, the efficiency appears to peak after the first hour and subsequently decrease. Since copper is electro-deposited at the same time as ammonia synthesis, the reported faradaic efficiency

is actually an overestimation of the system efficiency to produce ammonia. This stagnation in performance can potentially be explained by both hypotheses. Hypothesis 1 suggests oxygen vacancy sites to be an active component for ammonia synthesis, and since the hydroxide ion concentration is increasing with time, these sites may become neutralized as time increases. As for Hypothesis 2, it is likely that depositing copper past the optimal amount during the synthesis of ammonia causes a decrease in the yield. One study looked at this very relationship[21], in which they electro-deposited copper in an acidic solution for 2, 10, 30, and 60 minutes (Cu-2 to Cu-60; Figure 4.8) on carbon paper. An inverse relationship was found between the NH_3 rate/efficiency and the copper deposition time. The authors concluded that there is an optimal copper thickness because the thickness can alter the local concentration of the reactant species. With a shorter copper thickness, more nitrogen is thought to occupy the vicinity of the active sites, which address the common issue of high hydrogen adsorption on these catalysts. Thus, the time-dependency results do not outwardly refute either of the two hypotheses.

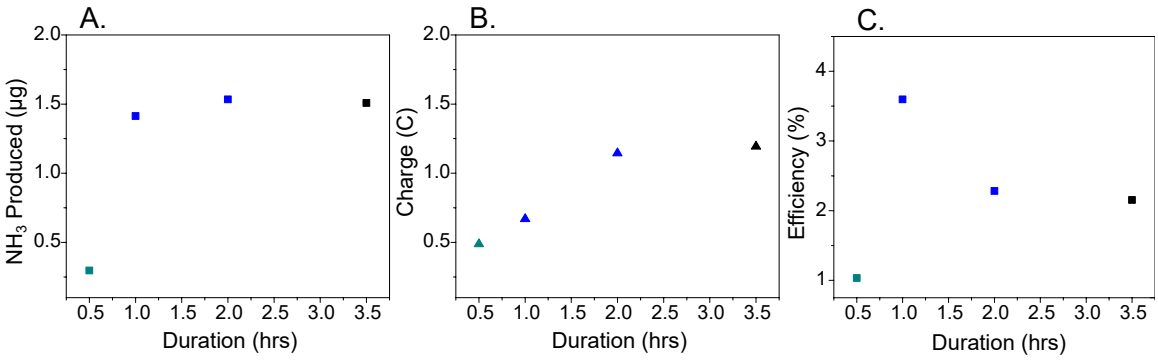

Figure 4.9: Time dependency results for (A.) NH_3 produced (μg), (B.) Charge and (C.) Efficiency, with each color representing a different sample. A potential of 0.1V vs RHE (-0.571V vs Ag/AgCl) is used for all of the experiments

As for the voltage dependency plot (Figure 4.10) a clear trend emerges, which shows that the amount of ammonia increases as the potential becomes more positive. An optimal voltage was not investigated for this study by applying more positive potentials past 0.1V vs RHE; however, these experiments do illustrate that attempting to apply potentials similar to other catalysts in literature results in a drastic decrease in the production of ammonia.

Hypothesis 1, which suggests the active site to be the oxygen vacancies of VO_2, does not account for the large difference in the potential applied to those applied in literature. Specifically, one study[18] (Table 4.3 intentionally made a multi-valent (+5 and +4 oxidation state) vanadium oxide material to act as their catalyst for ammonia synthesis. This catalyst

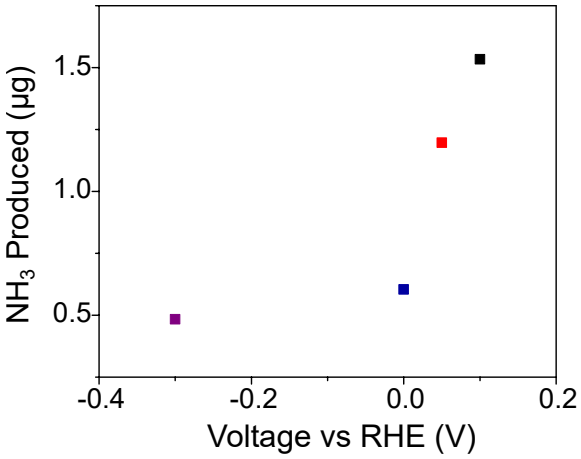

Figure 4.10: NH_3 produced (μg) voltage, with each color representing a different sample. Voltage dependency data are taken from 2-hour long experiments

managed to operate at a lower potential (-0.35V vs RHE) than all of the other vanadium oxide studies, which the authors attribute to the high concentration of oxygen vacancies that significantly decreased the nitrogen adsorption energy. Even though this study does show a decrease in the optimal potential due to oxygen vacancies, it is still 450 mV more negative than the applied potential of 0.1V. Thus, based on these results it is most likely that copper provides the active sites for nitrogen reduction in our electrode (Hypothesis 2) and not the vanadium oxide catalyst (Hypothesis 1).

The clear question remains as to how the VO_2 (AA) and RGO catalyst outperforms all of the controls if they are all introduced to copper ions during the acidification step in 0.5M H_2SO_4. To answer this question, cyclic voltammetry and linear sweep voltammetry are implemented. Both of these techniques can describe the faradaic and non-faradaic events that occur on the electrode. Figure 4.11 shows the results of the cyclic voltammetry experiment performed in nitrogen and 0.5M $LiClO_4$ (pH=8) with $Cu(ClO_4)_2$-$6H_2O$ added to the electrolyte. Specifically, Figure 4.11B plots the voltage corresponding to the highest and most

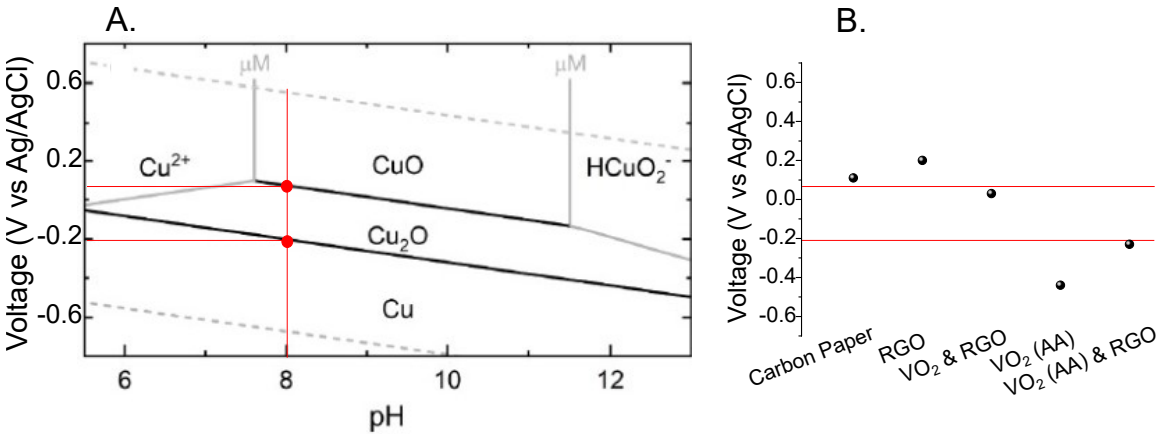

Figure 4.11: A. Simplified Pourbaix diagram for copper[22]; B. Potential for the highest and most defined copper reduction peak for each catalyst

defined copper reduction peak for each of the catalysts. This result shows that the copper ions are mostly reduced to Cu_2O for the bare carbon paper, RGO, and VO_2 & RGO samples (≈0.75V vs Ag/AgCl). However, the VO_2 (AA) & RGO sample has a reduction peak similar to where Cu_2O is reduced to copper metal (≈ -0.2V vs Ag/AgCl). At the applied potential for electrocatalysis (-0.571V vs Ag/AgCl), both of the aforementioned reduction potentials are surpassed and so copper is initially thought to be be fully reduced. Given that the VO_2 (AA) & RGO sample visibly reduces more copper than the other catalysts during ammonia synthesis, it is likely that this catalyst alters the surface dynamics related to reducing copper from its oxidized state.

Electrodes that underwent ammonia synthesis were later analyzed using linear sweep voltammetry. These voltammograms (Figure 4.12) serve to further illustrate the surface species on the electrode. All of the peaks that show up near 0.17V and 0.37V vs Ag/AgCl in Figures 4.12A and B are due to phases of oxidized copper, particularly $Cu(OH)_2$ and CuO. This is confirmed by the oxidation of the electro-deposited copper electrode (Figure 4.12C and D) which shows two distinct oxidation peaks for copper, the same peaks that appear in a study[137] that performed cyclic voltammetry experiments of copper in an alkaline environment. When comparing the 1st and 4th scan for each catalyst, only one distinct peak appears near 0.9V vs Ag/AgCl for VO_2 (AA) with RGO or 3wt%Fe. The peak dissipates

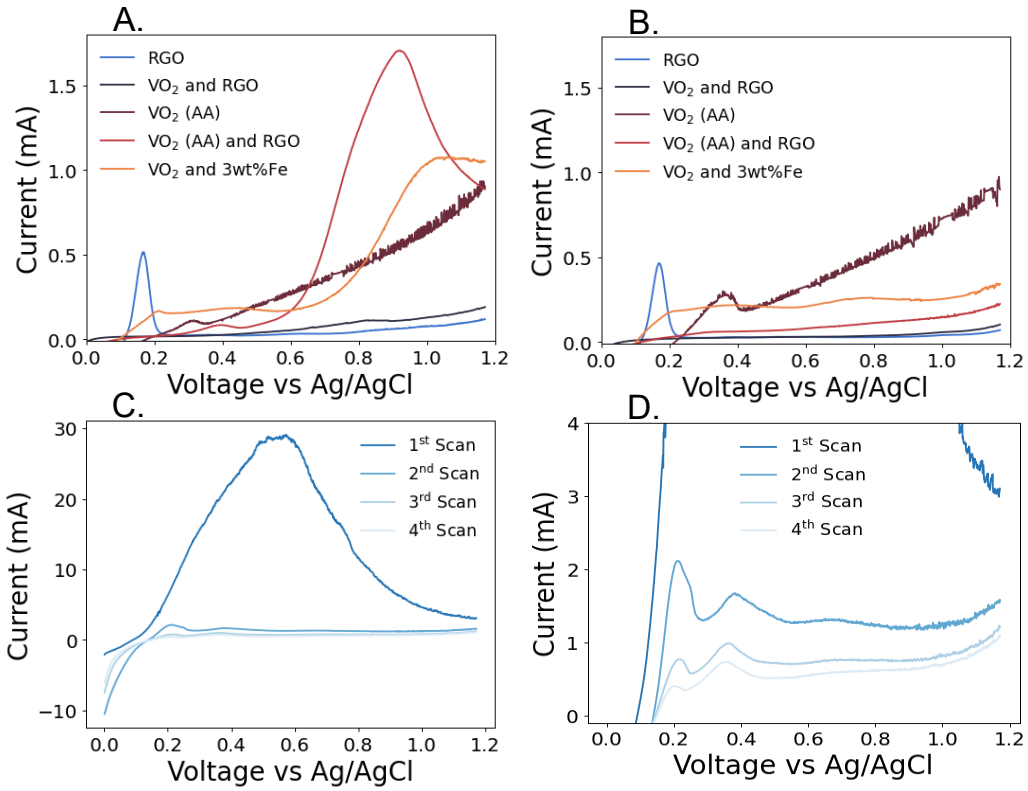

Figure 4.12: Linear sweep voltammograms (A. 1^{st} and B. 4^{th} scan) of catalysts post-electrochemical ammonia synthesis obtained in Ar; C./D. LSV scans of electro-deposited (charge passed=2C) copper control sample obtained in Ar

after the first scan, and doesn't result in a subsequent increase in any of the other peaks. Given that this peak appears only for the catalysts that synthesized a significant amount of ammonia, it is likely that it is due to an adsorbate related to ammonia synthesis. However, the true nature of this peak is yet to be identified in this study. There is precedence in the literature for a Cu_2O_3 phase of copper that has a peak near 0.94V vs Ag/AgCl, but it typically appears in a strong base solution.[138] As well, the peak does not appear in the previous cyclic voltammetry experiments in argon or nitrogen. Despite not knowing the nature of this peak, it is still important to note that all peaks for the VO_2 (AA) & RGO sample are fully dissipated by the 4th scan, while strong copper oxide peaks remain for all of the other samples (besides VO_2 (AA) & RGO). This is indicative of metallic copper being fully oxidized and dissolving into solution. Therefore, the results indicate that the

VO_2 (AA) & RGO sample is able to successfully reduce copper metal during the ammonia synthesis process.

Beyond the scope of this study is the consideration of another element that may have influenced the synthesis of ammonia. Since a lithium salt was used as the electrolyte, there is the possibility of forming lithium nitride on the working electrode. Metallic lithium has a great ability shared by few elements (e.g. Fe and Ru) to dissociate dinitrogen molecules (N_2) into two adsorbates (*N and *N); while lithium nitride (Li_3N) reacts easily in water to form lithium hydroxide and ammonia. In this project, SEM-EDS revealed nitrogen in the same location as the copper deposits, which could be due to Li_3N (Figure A.7). As well, one experiment showed that an electrode that underwent electrocatalysis in nitrogen first and later tested in argon yielded similar amounts of ammonia. This supports the EDS results, indicating that nitrogen remained on the electrode. Copper has recently been identified as a promoter of lithium nitridation to form Li_3N in a glovebox, decreasing the synthesis time from days to minutes.[101] Another study[100] used a high-surface area, copper electrode for ammonia synthesis because copper does not form an alloy with lithium. This allowed them to reduce nitrogen, form lithium nitride, and systematically synthesize ammonia. Studies that follow this "lithium-mediated" synthesis approach operate at very negative potentials close to the reduction of Li^+ and operate at pressures above atmospheric. However, there are studies[139,140] that operate under ambient conditions and mention the possibility of having lithium nitride that enhanced the synthesis rate. In general, the field could benefit from attaining *in-situ* characterization on Li_3N during electrocatalysis to identify its stability in aqueous systems.

4.4 Conclusion

For the first time, an ascorbic acid-treated VO_2 catalyst is implemented in an electrochemical setup, and when coupled with RGO, plays an integral part in reducing copper and nitrogen to synthesize ammonia. The task of reducing copper and nitrogen proves to be

non-trivial in an alkaline environment where multiple phases of copper oxides can exist based on the applied potential and the electrode surface dynamics. Two hypotheses are considered to explain the preferred synthesis of ammonia on VO_2 (AA) & RGO; the first hypothesis stating that oxygen vacancies on VO_2 (AA) act as the primary active site for ammonia synthesis, while the second hypothesis states that copper is the active site and VO_2 (AA) & RGO mainly serves to reduce copper ions readily on carbon paper. The second hypothesis is ultimately chosen to explain the electrode performance because (1) the potential applied for ammonia synthesis is closest to that of copper nanoparticles and not of vanadium oxide particles from literature; (2) the stagnation in ammonia synthesis beyond 1 hour can be due to the simultaneous over-deposition of copper; and (3) the voltammetry results show that the VO_2 (AA) & RGO catalyst reduces copper ions to copper metal, while the control samples retain copper oxide species.

To improve upon the nitrogen reduction reaction using vanadium oxides, it would be beneficial to investigate a mixed-valent (+5, +4) vanadium oxide catalyst, given that one study[18] achieved a yield that is more than an order of magnitude higher than all of the other vanadium oxide catalysts previously studied. To that end, coupling copper nanoparticles with a mixed-valent vanadium oxide could potentially reduce the optimal electrochemical potential and improve upon the ammonia synthesis rate. Production of ammonia may also benefit from flowing in a small percentage of hydrogen with nitrogen into the electrolyte to account for the increase in hydroxide concentration during ammonia synthesis. Finally, future studies into the copper and nitrogen reduction mechanisms would greatly benefit from *in-situ* characterization techniques, such as *in-situ* FTIR to identify surface intermediate species.

CHAPTER 5

Conclusions and Future Directions

The studies presented in this dissertation highlighted the performance of two solid-state electrolytes for intermediate ammonia synthesis, and the performance of an electrically conductive phase of VO_2. In Chapter 2, a perovskite proton conductor was synthesized and implemented into a double chamber reactor to electrochemically synthesize ammonia. It is found that this proton conductor performed just as well as other proton conductors when using steam as the proton source; however it is revealed that the perceived ammonia yields are ambiguous and therefore steam is not a viable proton source for electrochemical ammonia synthesis. Chapter 3 delved into synthesizing and implementing sodium/potassium solid electrolytes, particularly to take advantage of the NEMCA effect. It is revealed that ammonia is consistently synthesized in a non-stoichiometric concentration of hydrogen and that potassium outperforms sodium electrochemical promotion. Finally, Chapter 4 shifts focus from the electrolyte to the catalyst, where a vanadium oxide catalyst is synthesized and used to synthesize ammonia electrochemically. This project showed that the designed catalyst is able to simultaneously reduce copper and nitrogen in an alkaline environment to form ammonia.

All of the studies presented in this dissertation can be further improved upon in future studies with the goal of increasing the rate and efficiency of ammonia synthesis. As mentioned in Chapter 2, formal experiments using the same proton conducting electrolyte and with pure hydrogen gas at the anode can greatly improve the electrocatalysis. Beyond changing the system conditions, the fabrication of the electrochemical cell can be optimized by decreasing the electrolyte thickness. Decreasing the electrolyte thickness to a few micrometers can greatly reduce the ionic resistance of the cell and may reduce the optimal potential for ammonia synthesis. As for the sodium/potassium electrolyte study

in Chapter 3, further fundamental insights can be made regarding the surface intermediates found on the working electrode. Temperature programmed desorption (TPD) and *in situ* DRIFTS analysis are proven techniques for analyzing the NEMCA effect for other reactions, and would prove useful to assessing what adsorption species are present during ammonia synthesis. Lastly, for the vanadium oxide catalyst study discussed in Chapter 4, there are several lingering questions that can be answered with further experiments. For instance, XPS can be used to ascertain whether lithium nitride is formed during the process of synthesizing ammonia. As well, *in-situ* spectral techniques like FTIR can identify the state of copper at different points of the synthesis process. In terms of increasing the yield of ammonia, this may be achieved by coupling an optimal amount of copper with a multi-valent vanadium oxide catalyst, the latter catalyst of which is shown in literature to perform relatively well.

Appendix A

A.1 Supplementary Figures for Chapter 3

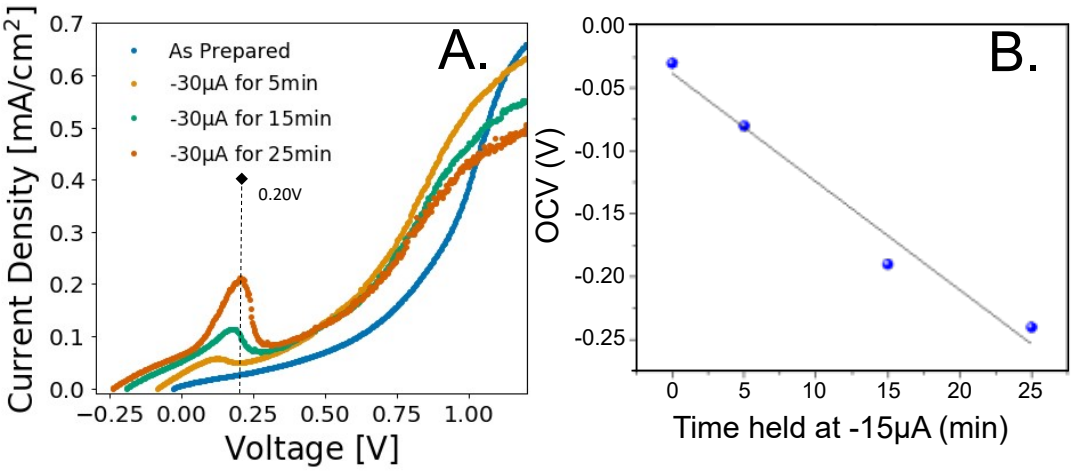

Figure A.1: (A.) Linear sweep voltammograms and (B.) Open-circuit potential taken after the working electrode is held at -30μA for different time periods in N_2 flow

A.2 Supplementary Figures for Chapter 4

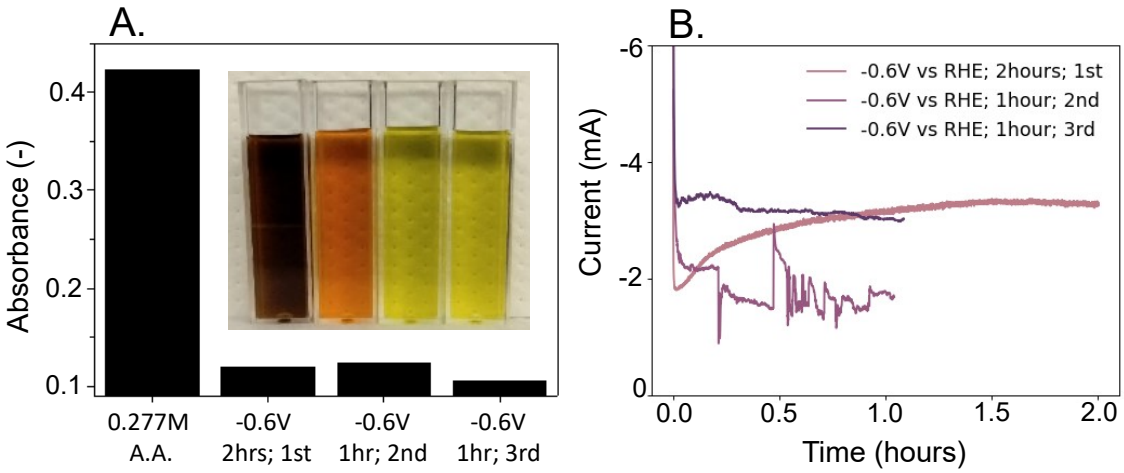

Figure A.2: A. Absorbance values taken at a wavelength of 655 nm of bulk 0.277M ascorbic acid solution and for three pre-electrolysis steps; B. Pre-electrolysis performed at -0.6V vs RHE in Ar-saturated 0.05M H_2SO_4 performed three times

When the VO_2 (AA) and RGO catalysts first underwent the ammonia synthesis process in 0.05M H_2SO_4 and in argon (Figure A.2), an odd reddish color appeared during the Berthelot reaction to make indophenol. A reddish-hue is indicative of forming indophenol red (pH: 6.5) which is more acidic than indophenol-blue (pH: 10-12).[141,142] The cause of this color change is ascribed to ascorbic acid seemingly remaining on the VO_2 particles and leaching into the electrolyte, despite the numerous washing steps. Thus, to reach a normal baseline for subsequent experiments, i.e removing the ascorbic acid, all electrodes undergo a pre-electrolysis step at -0.6V vs RHE in 0.05M H_2SO_4 for roughly 4 hours total. As is shown in Figure A.2B, the current after the final pre-electrolysis step is similar to the first step, which shows that the electrode retains its electrochemical properties after ascorbic acid is removed.

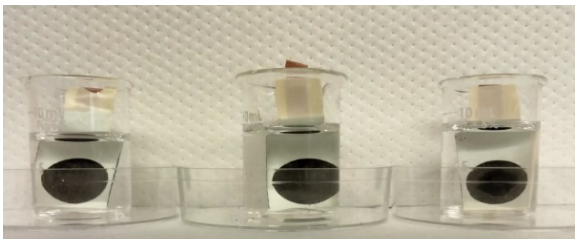

Figure A.3: Acid treatment of electrodes in 0.05M H_2SO_4 for 48 hours

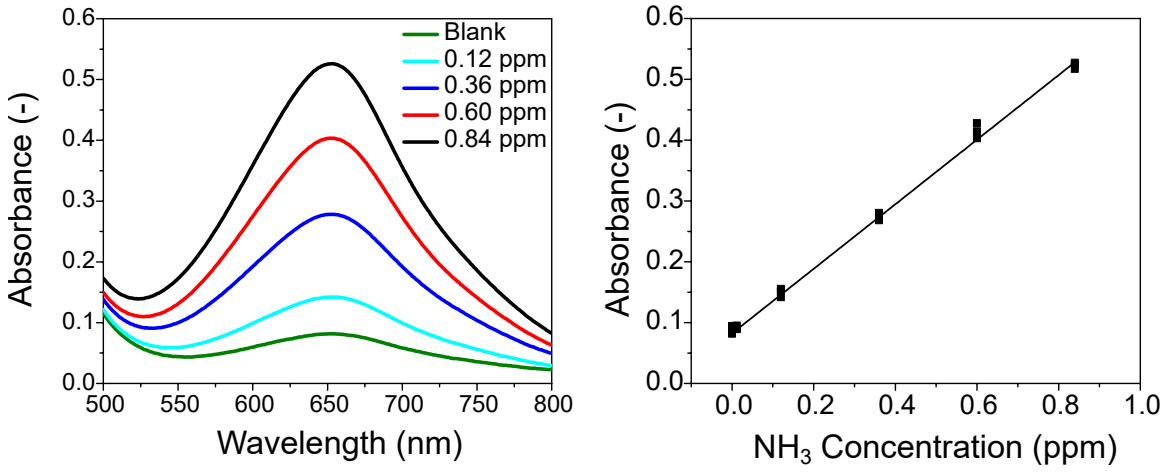

Figure A.4: Calibration curve for ammonia detection using indophenol for a 0.5M $LiClO_4$ electrolyte

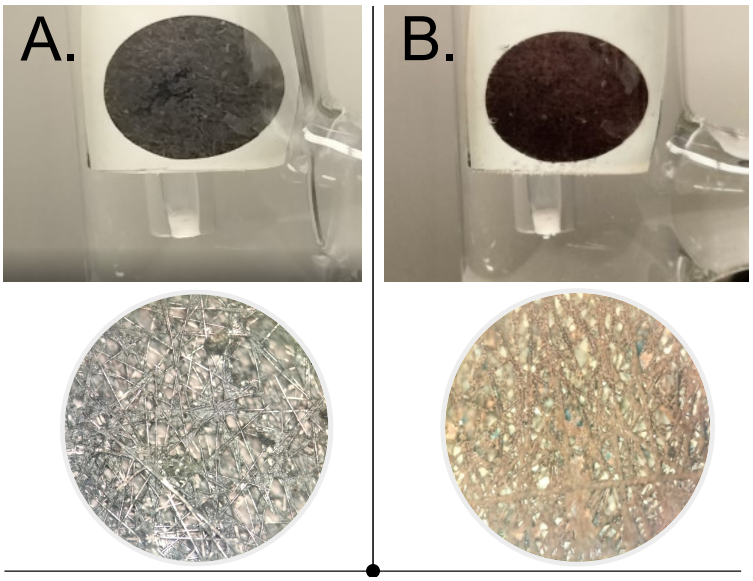

Figure A.5: Optical images (20x) of VO_2 (AA) & RGO (A.) at t= 0min and (B.) at t= 2hrs

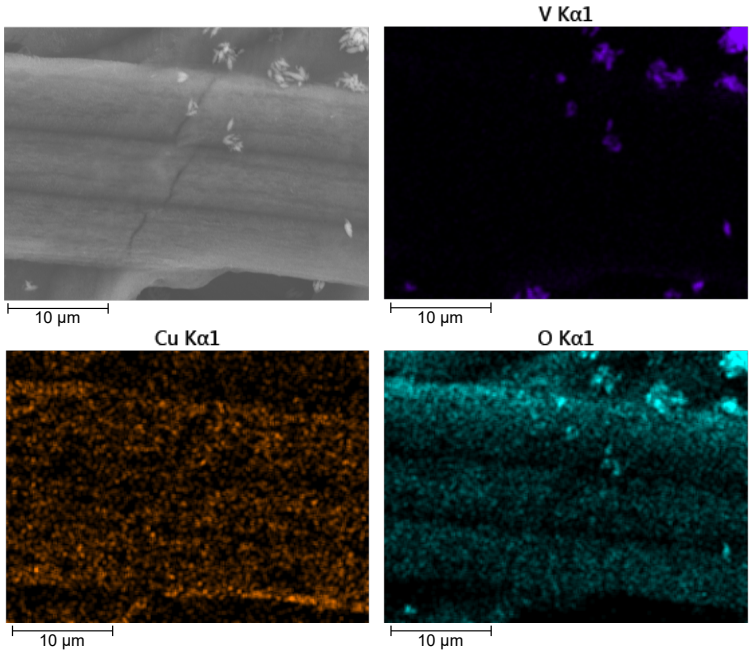

Figure A.6: SEM-EDS images of VO_2 (AA) & RGO on carbon paper, and showing copper, oxygen and vanadium map

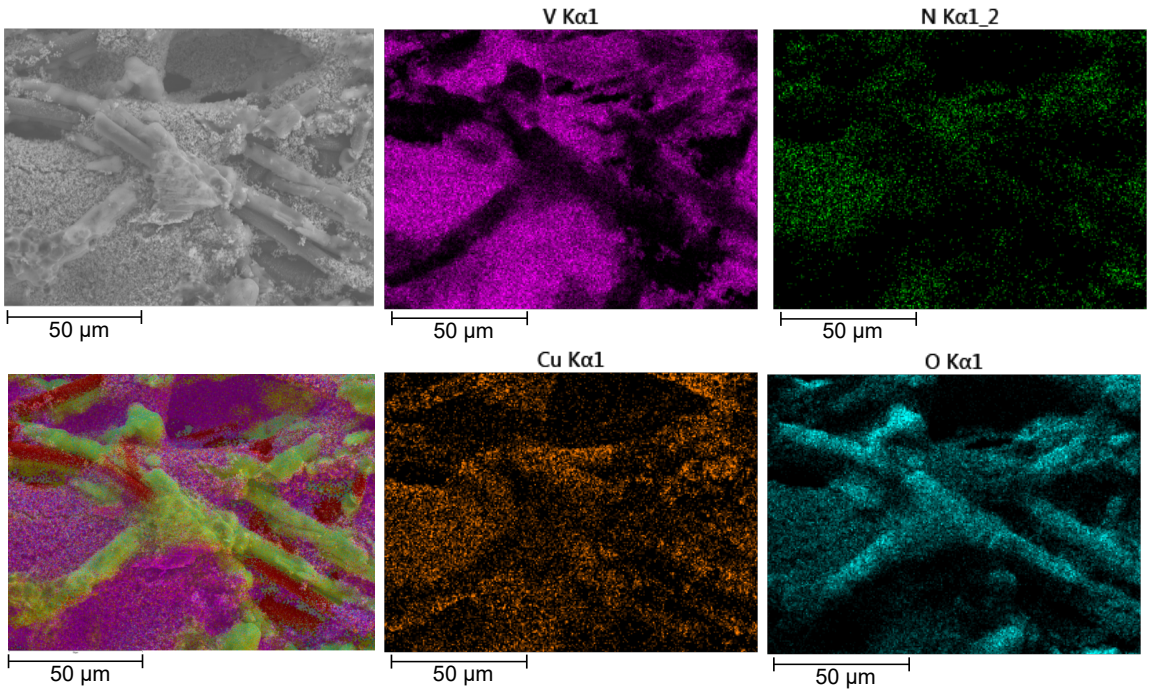

Figure A.7: Additional SEM-EDS images of VO_2 (AA) & RGO on carbon paper, and showing copper, nitrogen, oxygen, and vanadium map

A.3 Comparing VO_2 Oxide Performance for NH_3 Synthesis

A.3.1 Methods

A.3.1.1 Catalyst Synthesis

Vanadium dioxide particles are produced the same way described in Chapter 4. The catalyst inks are prepared by mixing together 960 μL of IPA/H_2O (1:1 vol), 40 μL of Nafion, and 10 mg of catalyst. The ink is sonicated for 2-3 minutes and drop cast onto a 1cm^2, acid-cleaned MGL190 carbon paper electrode. The carbon paper electrode is cleaned by cycling in 1E-3M H_2SO_4 for 100 cycles in the voltage window of 0 to 1.125V (vs Ag/AgCl), and at a rate of 200 mV/s. After cleaning, the electrode is dried in a desiccator for 5 minutes and then 20 μL of the catalyst ink is drop cast onto the carbon paper. The electrode is dried one last time in a desiccator, after which it is used for electrochemical experiments.

A.3.1.2 Characterization

The catalysts are characterized using x-ray diffraction (XRD) using a Cu K-α source and acquiring spectra within a 2θ range of 10 – 80 degrees. Scanning electron microscopy is then used to evaluate the morphology of each catalyst. Electrochemical measurements for catalyst characterization are performed in a beaker cell using cyclic voltammetry and linear sweep voltammetry on a CHI 660 potentiostat/galvanostat. These electrochemical methods are performed in 25mL of 0.1M Na_2SO_4 electrolyte using a graphite rod as the counter electrode, Ag/AgCl reference electrode, and the drop-cast CP as the working electrode. Cyclic voltammetry is performed to ascertain the electrochemically active surface area (ECSA) using the double-layer capacitance method. Beginning with a negative polarization, 10 full cycles are obtained within 0 and -0.265V vs Ag/AgCl under a saturated argon environment. The positive current at -0.13V is taken and plotted as a function of the scan rate (at scans of 5, 10, 15, 20 and 25 mV/s). The linear sweep voltammetry method is used to provide polarization curves with which to further compare the different catalysts. The voltage is once again swept under negative polarization in the voltage window of 0 to -1.2V vs RHE. Scans are run at least twice in argon before running in nitrogen.

Preliminary nitrogen reduction reaction (NRR) experiments are conducted in a beaker cell at a selected voltage (e.g. -0.1V vs RHE) for 2 hours under nitrogen flow (20 sccm). Control experiments are performed for 30 minutes each just prior to the NRR. This involves argon flowing through the system at the open circuit voltage (OCV) and at the applied voltage for 30 mins respectively, along with nitrogen flow at OCV. For each control as well as for the NRR, 2mL aliquots of the electrolyte are taken out and used in the Berthelot reaction to evaluate the concentration of ammonia. Two milliliters of fresh electrolyte are replaced after each aliquot is removed in order to maintain the total volume of 25 milliliters. The rate and efficiency of ammonia formation are evaluated using equations 1 and 2.

$$Rate_{NH_3}(\frac{\mu g_{NH_3}}{mg_{cat} * h}) = \frac{M_g * V}{m * t} \tag{A.1}$$

$$\eta_{NH_3}(\%) = 100 * \frac{M_{mol} * V * 3 * F}{17 * C} \tag{A.2}$$

Where **Mg**: mass concentration of ammonia produced (μg/L); **V**: volume of electrolyte (L); **m**: mass of catalyst (mg); **t**: duration of NRR experiment (h); $\mathbf{M}_{mol}$: mol concentration of ammonia produced (mol/L); **F**: faraday's constant; **C**: charge passed during NRR (coulombs)

A.3.1.3 Results

The X-ray diffraction spectra for the catalysts (Fig A.8 A. and B.) confirms the synthesis of orthorhombic V_3O_7-H_2O, monoclinic VO_2 (using 5, 15, and 20mmol vanadium precursor), and a VO_2 (A) phase (using 25mmol vanadium precursor) that is an intermediary phase between monoclinic and rutile. As well, the spectra for VO_2 20mmolV doped with 3mol% tungsten appears to be rutile, although there should be an additional peak near 64.5 degrees. Lastly, XRD confirms the expected phase is achieved for each of the supports (Fig A.8 C.). Specifically, CeO_2 has the expected fluorite phase, γ-Al_2O_3 has a spinel structure, and $BaZr_{0.4}Ce_{0.4}Y_{0.1}Yb_{0.1}O_3$ has a cubic perovskite structure.

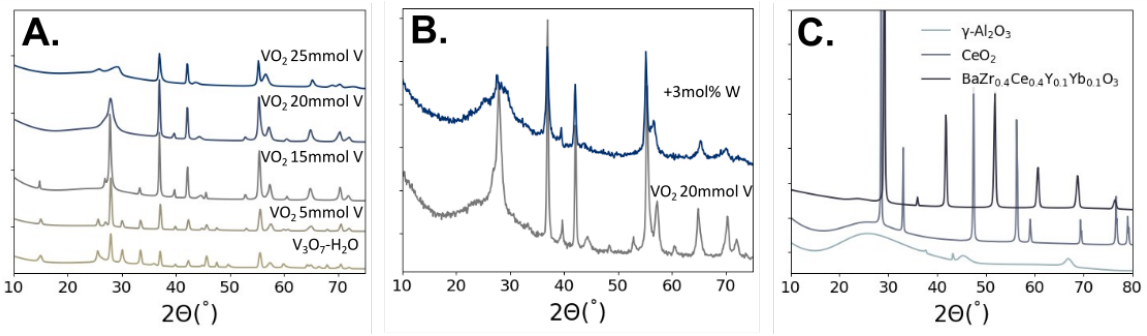

Figure A.8: X-ray diffraction spectra corresponding to (A.) the synthesized vanadium oxide catalysts, (B.) VO_2 20mmolV with and without 3mol% tungsten dopant, and (C.) the proposed support material

Scanning electron microscopy (SEM) reveals the morphologies of the catalysts, which are dependent on the initial V_2O_5 precursor concentration (Fig A.9). For the 15mmolV precursor, asterisk and snowflake morphologies are produced that have arms spanning 1-2μm.

As for the 20mmolV precursor, a consistent asterisk morphology is produced having arm spans of 1 µm. Dr. Aaron Daniel, who developed the hydrothermal synthesis methods used in this work, noted that the asterisk arms maintain the monoclinic phase within the core, but the outer edge is amorphous. When a much smaller amount of V_2O_5 was used (3 and 5 mmolV) then V_3O_7-H_2O was also produced in addition to VO_2 (Fig A.10). The resulting electron micrographs illustrate that nanobelts (3mmolV precursor) and bulk particles (5mmol V) are formed for V_3O_7-H_2O. All further characterization and NRR experiments for V_3O_7-H_2O are performed using the bulk particles.

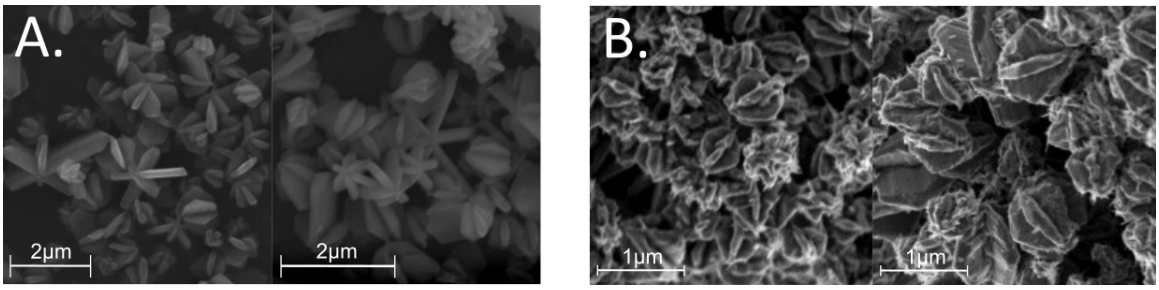

Figure A.9: SEM images of vanadium dioxide particles made using (A.) 15mmol vanadium and (B.) 20mmol vanadium precursor

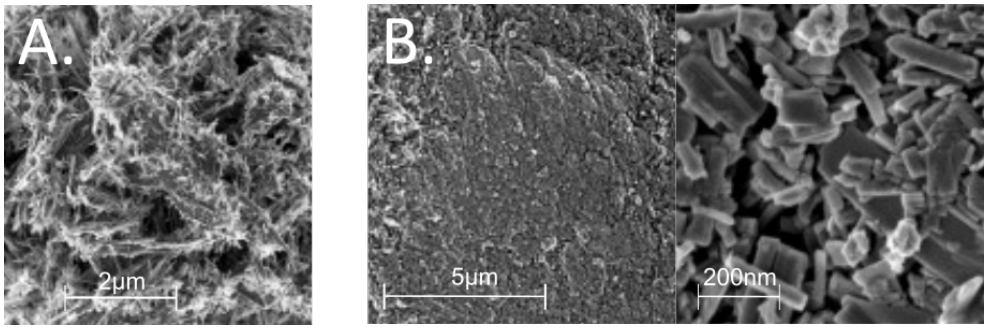

Figure A.10: SEM images of V_3O_7-H_2O particles made using (A.) 3mmol V_2O_5 and (B.) 5mmol V_2O_5

Using the double layer capacitance method to evaluate the ECSA (Fig A.11), the V_3O_7-H_2O catalyst displays the highest capacitance of 5.57 mF. This coincides with a study[136] that also applied V_3O_7-H_2O as a catalyst for electrochemical nitrogen reduction, in which they had a maximum capacitance of 3.05mF. The VO_2 catalysts made with 15mmolV and 20mmolV have similar capacitances, but when the 20mmolV catalyst is doped with 3mol%

tungsten the capacitance increased slightly from 0.40mF to 0.70mF. This could be due to the smaller resistance of the doped VO_2 or it may be due to the smaller size of these particles leading to increased active surface area. One study [105] that implemented VO_2 microspheres as catalysts achieved a capacitance of 5.6 mF. This is much higher that what we measured for the VO_2 catalysts, but it may be due to the preparation of the carbon electrode. Preliminary measurements on VO_2 catalysts supported on flame-treated carbon paper (not shown here) instead of the acid-cleaned ones displayed greatly improved capacitances near 2mF.

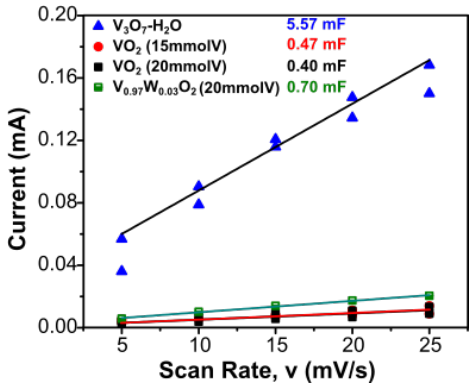

Figure A.11: Capacitive current density at -0.13V vs scan rate for different vanadium oxide-based catalysts

Linear sweep voltammetry is used to produce polarization curves of the catalysts. At the relevant voltages for the nitrogen reduction reaction (-0.1V to -0.7V vs RHE; Fig A.12), the VO_2 15mmolV and 20mmolV catalysts exhibited slightly higher current than the MGL 190 carbon paper. However, the V_3O_7-H_2O catalyst had nearly the same current as the carbon paper. It is expected that the catalysts would have a higher cathodic current than the carbon paper if they successfully synthesize ammonia. At even higher voltages (above -0.8V vs RHE), the V_3O_7-H_2O catalyst attains the highest current. This voltage window is where the hydrogen evolution reaction (i.e. HER) tends to dominate over the NRR for these catalysts. Thus, the HER reaction may be prominent on V_3O_7-H_2O at these higher potentials. In fact, another vanadium oxide hydrate, $V_{10}O_{24}$-H_2O was identified as an effective HER catalyst in an acid electrolyte. [143] Overall, the currents obtained by the catalysts correlate well with those achieved by similarly studied vanadium oxide catalysts.

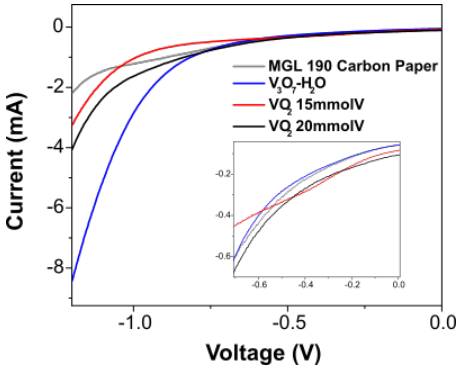

Figure A.12: Polarization curves of vanadium oxide catalysts exposed to saturated nitrogen gas

Catalyst	Potential (V)	Rate ($\mu g_{NH_3}/mg_{cat} * h$)	Efficiency (%)
V_3O_7-H_2O	-0.1	0.312	0.019
VO_2 20mmolV	-0.1	1.501	0.026
VO_2 25mmolV	-0.6	0.494	0.002

Table A.1: NRR results using vanadium oxide catalysts

The nitrogen reduction reaction experiments (at -0.1V or -0.6V) revealed that the catalysts produced a quantifiable amount of ammonia relative to control experiments. In addition to the argon control experiments that were run for each sample, an additional control was performed on a bare MGL190 carbon paper. At a potential of -0.1V (Fig A.13 A.), the bare carbon paper did not yield any ammonia. The ammonia synthesis rates (Table A.1) increase in the order: VO_2 20mmolV (Fig A.13 C), V_3O_7-H_2O (Fig A.13 B), and VO_2 25mmolV (Fig A.13 D). The highest rate obtained by the VO_2 20mmolV catalyst, 1.501 $\mu g_{NH_3}/mg_{cat}$*h, is roughly an order of magnitude smaller than a study that used VO_2 microspheres as a catalyst.

The low performance is potentially due to the catalysts having the semiconductor monoclinic phase instead of the metallic rutile form of VO_2. At the low potential of -0.1V, it is unlikely that the opposing hydrogen evolution reaction (HER) would dominate over nitrogen fixation. Thus, it is more likely that the VO_2 (M) phase catalysts were not electrically conductive enough to facilitate the proton-coupled transfer. The V_3O_7-H_2O catalyst also

underperformed, having the lowest rate of 0.312 $\mu g_{NH_3}/mg_{cat}$*h. A study that implemented V_3O_7-H_2O nanobelts[136] attained a rate roughly 50x higher than what we measured. In this case, the lower rate may be due to using bulk particles instead of the nanobelt morphology.

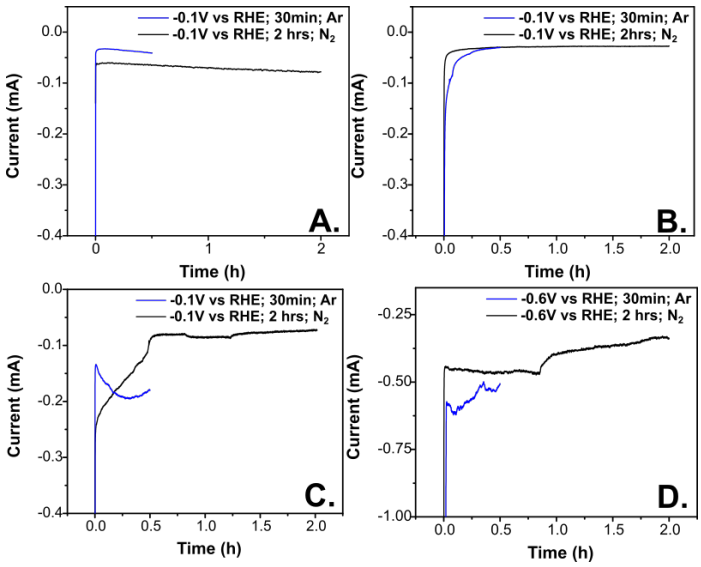

Figure A.13: Current response for NRR using (A.) Bare MGL190, (B.) V_3O_7-H_2O, (C.) VO_2 20mmolV, (D.) VO_2 25mmolV

A.4 Ammonia Detection using Indophenol

A reliable method of detecting ammonia is crucial in the field of electrochemical ammonia synthesis, particularly because the yield is relatively small and there are many factors that can influence this measurement. Many published results may be inaccurate simply because their ammonia determination method overestimates the actual concentration[141]. Greenlee et al. provided an extensive overview into ambient ammonia's influence on the resulting formation rate and efficiency, including how ammonia's basicity causes it to adhere to most surfaces (e.g. reactor chamber, gas flow tubes, and beakers)[144]. They highly suggest the use of adequate and extensive controls to monitor ambient ammonia, and to use these controls to more appropriately report on ammonia synthesized electrochemically. The controls that are mentioned involve repeatedly measuring ammonia concentration under different circumstances, such as under argon flow and with/without an applied voltage. To adequately

report on the amount of ammonia electrochemically produced, an ammonia determination technique first needs to be established.

Several methods exist for the purpose of determining the concentration of ammonia including: ion selective electrode (ISE), mass spectroscopy, gas chromatography, and spectrophotometry; although ISE and spectrophotometry are most easily accessible. There also exists a titration method that is fairly accurate, but isn't commonly used due to its low resolution (about 5 ppm)[145]. In the ISE method, an electrode resides at a certain voltage after placing it in a solution containing ammonium ions, and since the voltage is directly related to the logarithmic activity of ammonia, the concentration is then ascertained.

For the ISE and spectrophotometry methods, standard concentrations are used in order to obtain a linear fit. The linear fit enables the detection of ammonia by interpolating between points of known concentrations. In the spectrophotometry method, the linear relationship between absorption and concentration is due to the well known Beer-Lambert law. This law is effective up to a certain point, since a solution's rise in concentration results in a darker shade (higher absorption). Since the absorbance depends on light that is transmitted through the sample, a solution that absorbs light extremely well will not give accurate results. This is not particularly concerning for electrochemical devices since they do not yet produce ammonia near this value; and large absorbance peaks can also be circumvented through dilution.

For spectrophotometric detection of ammonia, the main methods fall under Nessler and Indophenol Blue. The indophenol blue reaction involves combining the analyte (ammonia), a hypochlorite solution, and phenol that gives off a bluish-green hue. Other reagents are typically added in order to make the method more reproducible; for instance, citrate solutions are added to prevent the formation of hydroxide precipitation[146]. A catalyst is also typically employed so as to increase the rate of reaction. Common catalysts include sodium nitroprusside and potassium ferrocyanide, and although the intricate reaction mechanisms aren't fully understood for these catalysts, they are still widely used and are fairly accurate.

The indophenol blue method has been performed using various phenolic compounds. This method was first developed using phenol salt, but phenol is a rather toxic compound which is why safer compounds have been implemented. Salicylic acid is one of the most used replacement for phenol, and has proven to be useful in the determination of ammonia[23]. The ammonia detection method used in this dissertation used salicylic acid to avoid the use of toxic phenol.

A.4.1 Methods

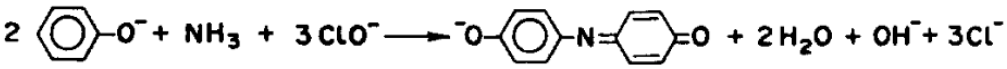

Figure A.14: Reaction steps to forming indophenol; figure reproduced with permission from Verdouw *et al.*[23]

The indophenol blue method performed using phenol or salicyllic acid results in the same bluish-green hue. Similarity between the two methods can also be seen from their reliance on three main components: a catalyst, active chlorine, and a phenol containing compound. The reaction, as shown in Figure A.14, occurs by first forming monochloramine from ammonia and active chlorine ions. Then the monochloramine reacts with the phenolic compound to form an intermediate benzoquinone monoimine[147], known widely as indophenol blue.

A.4.2 Indophenol Blue Method: Salicylic Acid

Most methods implementing salicylic acid do so indirectly through the use of a sodium salicylate salt. The reason why most researchers use sodium salicylate is because its solubility in water at room temperature (1250 g/mL) is much higher than that for salicylic acid (2g/L). When the sodium salicylate salt dissolves, it then produces salicylic acid and ionized sodium. In the present case, salicylic acid was used as opposed to sodium salicylate in following with the protocol established by[148]. The issue of salicylic acid's solubility was circumvented by partially neutralizing/dissolving it in sodium hydroxide. Since the pH of

the final solution has to be fairly basic (above a pH of 12) in order to form the indophenol, it is assumed that the researchers accounted for all of the sodium hydroxide used in the final solution.

The procedure for detecting ammonia starts with first making the following reagents: **Reagent A** consists of 5% salicylic acid and 5% trisodium cirate in 1 M NaOH; **Reagent B**: is a 0.05 M NaClO solution in DI water; **Reagent C**: is a 1% sodium nitroprusside dihydrate in DI water. First, 2 mL of analyte is taken from its source and put into a 15 mL centrifuge tube. The reagents are added to the analyte in quick succession: 2 mL of Reagent A, 1 mL of Reagent B, 200 microliters of Reagent C. The solution is agitated for a few seconds by shaking the centrifuge tube, and it then sits for 2 hours. Finally, the absorbance spectra is taken using a spectrophotometer in the UV-Vis range (800-300 nm^{-1}). To obtain a calibration curve, The absorption peak at 655 nm is taken and plotted against the ammonium ion concentration. Calibration curves are made for each electrolyte/acid trap solution that is used.

The sodium hypochlorite used to detect ammonia has a low shelf life, which means that its concentration needs to be ascertained periodically so that the moles of hypochlorite used in each test is consistent. To measure the concentration of hypochlorite in the stock solution, a titration technique known as iodometry is used. This process begins with making the following reagents: **Reagent A** is a 0.1 M sodium thiosulfate solution in DI water; **Reagent B** is a 10 g/L starch solution in DI water; and **Reagent C** consists of 0.8g potassium iodide (KI), 10mL of Reagent B, and 10 mL of acetic acid. Dilute solution to 200 mL with DI water. The first step is to fill a 25 mL burette with Reagent A up to the 0 mL graduation mark. Then add 5 mL of sodium hypochlorite and 20 mL of Reagent C into a beaker and stir using a magnetic stirrer. Then using the burette, add Reagent A drop-wise into the beaker until the solution in the beaker becomes clear. The total titration volume of Reagent A is recorded and is used to calculate the concentration of the hypochlorite stock solution.

Conducting blank measurements provides a baseline for future ammonia tests, limits the range of ammonia determination, and also serves as a way of checking that reagents are viable. For Chapters 2 and 3, the ”blank” solutions were performed using its acid trap solution (0.001 M H_2SO_4), while Chapter 4's blank solution is its electrolyte (0.5M $LiClO_4$). These blank solutions follow the same procedure for ammonia quantification and are prepared for every electrochemical test.

References

[1] J. W. Erisman, M. A. Sutton, J. Galloway, Z. Klimont and W. Winiwarter, *Nature Geoscience*, 2008, **1**, 636–639.

[2] S. Giddey, S. Badwal and A. Kulkarni, *International Journal of Hydrogen Energy*, 2013, **38**, 14576–14594.

[3] I. A. Amar, R. Lan, C. T. G. Petit and S. Tao, *Electrocatalysis*, 2015, **6**, 286–294.

[4] M. Liu, Y. Chen, L. A. Zhang, T. Wei and P. Yang, *Chemistry of Materials*, 2017, **29**, 1490–1495.

[5] S. J. Skinner and J. A. Kilner, *Review Literature And Arts Of The Americas*, 2003, **6**, 30–37.

[6] B. C. Steele, *Solid State Ionics*, 2000, **129**, 95–110.

[7] D. W. Strickler and W. G. Carlson, *Journal of the American Ceramic Society*, 1965, **48**, 286–289.

[8] K.-D. Kreuer, *Annual Review of Materials Research*, 2003, **33**, 333–359.

[9] S. Kishira, G. Qing, S. Suzu, R. Kikuchi, A. Takagaki and S. T. Oyama, *International Journal of Hydrogen Energy*, 2017, **42**, 26843–26854.

[10] S. Choi, C. J. Kucharczyk, Y. Liang, X. Zhang, I. Takeuchi, H.-I. Ji and S. M. Haile, *Nature Energy*, 2018, **3**, 202–210.

[11] G. M. CROSBIE and G. J. TENNENHOUSE, *Journal of the American Ceramic Society*, 1982, **65**, 187–191.

[12] F. Šimko, A. Rakhmatullin, P. Florian, M. Kontrík, M. Korenko, Z. Netriová, V. Danielik and C. Bessada, *Inorganic Chemistry*, 2017, **56**, 13349–13359.

[13] Y. Yin, Y. Li, S. Li, L. Chen, P. Zhai and G. Ye, 2017.

[14] X. Zhang, Q. Liu, X. Shi, A. M. Asiri, Y. Luo, X. Sun and T. Li, *Journal of Materials Chemistry A*, 2018, **6**, 17303–17306.

[15] G. F. Chen, X. Cao, S. Wu, X. Zeng, L. X. Ding, M. Zhu and H. Wang, *Journal of the American Chemical Society*, 2017, **139**, 9771–9774.

[16] Y. Song, T. Wang, J. Sun, Z. Wang, Y. Luo, L. Zhang, H. Ye and X. Sun, *ACS Sustainable Chemistry and Engineering*, 2019, **7**, 14368–14372.

[17] A. Liu, X. Liang, Q. Yang, X. Ren, M. Gao, Y. Yang and T. Ma, *ChemPlusChem*, 2021, **86**, 166–170.

[18] W. Fang, J. Zhao, T. Wu, Y. Huang, L. Yang, C. Liu, Q. Zhang, K. Huang and Q. Yan, *Journal of Materials Chemistry A*, 2020, **8**, 5913–5918.

[19] L. Hu, A. Khaniya, J. Wang, G. Chen, W. E. Kaden and X. Feng, *ACS Catalysis*, 2018, **8**, 9312–9319.

[20] X. Guo, W. Yi, F. Qu and L. Lu, *Journal of Power Sources*, 2020, **448**, 227417.

[21] C. Du, Y. Gao, J. Wang and W. Chen, *Chemical Communications*, 2019, **55**, 12801–12804.

[22] F. D. Speck and S. Cherevko, *Electrochemistry Communications*, 2020, **115**, 106739.

[23] H. Verdouw, V. Echteld and E. Dekkers, *Ammonia Determination Based on Indophenol Formation With Sodium Salicylate*, 2005.

[24] C. A. Fernandez, N. M. Hortance, Y.-H. Liu, J. Lim, K. B. Hatzell and M. C. Hatzell, *Journal of Materials Chemistry A*, 2020, **8**, 15591–15606.

[25] T. D. Kelly and G. R. Matos, *U.S. Geological Survey, 'Nitrogen (Fixed) — Ammonia Statistics'*, Last Modified: 03.30.2020, minerals.usgs.gov/minerals/pubs/historical-statistics/ds140-nitro.xlsx.

[26] S. Back and Y. Jung, *Physical Chemistry Chemical Physics*, 2016, **18**, 9161–9166.

[27] R. Hawtof, S. Ghosh, E. Guarr, C. Xu, R. M. Sankaran and J. N. Renner, *Asian Journal of Chemistry*, 2019, **31**, year.

[28] A. J. Martín, T. Shinagawa and J. Pérez-Ramírez, *Chem*, 2019, **5**, 263–283.

[29] C. A. Fernandez and M. C. Hatzell, *Journal of the Electrochemical Society*, 2020, **167**, 143504.

[30] V. Kyriakou, I. Garagounis, A. Vourros, E. Vasileiou and M. Stoukides, *Joule*, 2020, **4**, 142–158.

[31] D. Yi, S. Sanghvi, C. P. Kowalski and S. M. Haile, *Chemistry of Materials*, 2019, **31**, 9807–9818.

[32] S. M. Haile, G. Staneff and K. H. Ryu, *Non-stoichiometry, grain boundary transport and chemical stability of proton conducting perovskites*, 5, 2001.

[33] S. M. Haile, C. R. Chisholm, K. Sasaki, D. A. Boysen and T. Uda, *Faraday discussions*, 2007, **134**, 17–39.

[34] S. Sanghvi and S. M. Haile, *Solid State Ionics*, 2020, **349**, 115291.

[35] I. A. Amar, R. Lan, C. T. Petit and S. Tao, *Journal of Solid State Electrochemistry*, 2011, **15**, 1845–1860.

[36] S. Hossain, A. M. Abdalla, S. N. B. Jamain, J. H. Zaini and A. K. Azad, *Renewable and Sustainable Energy Reviews*, 2017, **79**, 750–764.

[37] I. Garagounis, V. Kyriakou, A. Skodra, E. Vasileiou and M. Stoukides, *Frontiers in Energy Research*, 2014, **2**, 1.

[38] J. Kim, S. Sengodan, S. Kim, O. Kwon, Y. Bu and G. Kim, *Renewable and Sustainable Energy Reviews*, 2019, **109**, 606–618.

[39] S. M. Haile, D. A. Boysen, C. R. Chisholm and R. B. Merle, *Nature*, 2001, **410**, 910–913.

[40] S. M. Haile, *Materials Today*, 2003, **6**, 24–29.

[41] C. R. Chisholm, D. A. Boysen, A. B. Papandrew, S. K. Zecevic, S. Cha, K. A. Sasaki, Á. Varga, K. P. Giapis and S. M. Haile, *Interface*, 2009, **18**, 53–59.

[42] G. Qing, R. Kikuchi, A. Takagaki, T. Sugawara and S. T. Oyama, *Journal of Power Sources*, 2016, **306**, 578–586.

[43] T. Matsui, T. Kukino, R. Kikuchi and K. Eguchi, *Journal of The Electrochemical Society*, 2006, **153**, A339–A342.

[44] C. R. I. Chisholm, D. a. Boysen, A. B. Papandrew, S. Zecevic and S. Cha, *From Laboratory Breakthrough to Technological Realization: The Development Path for Solid Acid Fuel Cells*, Fall, 2009.

[45] A. Paw, C. Pawlaczyk, B. Hilczer *et al.*, *Solid State Ionics*, 1990, **44**, 17–19.

[46] C. Ramasastry and K. S. Ramaiah, *Journal of Materials Science*, 1981, **16**, 2011–2016.

[47] K. Imamura and J. Kubota, *Sustainable Energy & Fuels*, 2018, **2**, 1278–1286.

[48] K. Sato, K. Imamura, Y. Kawano, S.-i. Miyahara, T. Yamamoto, S. Matsumura and K. Nagaoka, *Chemical science*, 2017, **8**, 674–679.

[49] Y. Yamazaki, F. Blanc, Y. Okuyama, L. Buannic, J. C. Lucio-Vega, C. P. Grey and S. M. Haile, *Nature materials*, 2013, **12**, 647–651.

[50] L. Malavasi, C. A. Fisher and M. S. Islam, *Chemical Society Reviews*, 2010, **39**, 4370–4387.

[51] K. D. Kreuer, *Aspects of the formation and mobility of protonic charge carriers and the stability of perovskite-type oxides*, 1, 1999.

[52] C.-H. Kim and C. D. Frisbie, *Journal of the American Chemical Society*, 2016, **138**, 7220–7223.

[53] A. Khorshidi, J. Violet, J. Hashemi and A. A. Peterson, *Nature Catalysis*, 2018, **1**, 263–268.

[54] M. A. Ardagh, O. A. Abdelrahman and P. J. Dauenhauer, *ACS Catalysis*, 2019, **9**, 6929–6937.

[55] G. Pitselis, P. Petrolekas and C. Vayenas, *Ionics*, 1997, **3**, 110–116.

[56] G. Marnellos, S. Zisekas and M. Stoukides, *Journal of Catalysis*, 2000, **193**, 80–87.

[57] C. Yiokari, G. Pitselis, D. Polydoros, A. Katsaounis and C. Vayenas, *The Journal of Physical Chemistry A*, 2000, **104**, 10600–10602.

[58] J. Díez-Ramírez, V. Kyriakou, I. Garagounis, A. Vourros, E. Vasileiou, P. Sánchez, F. Dorado and M. Stoukides, *ACS Sustainable Chemistry & Engineering*, 2017, **5**, 8844–8851.

[59] K. Kreuer, W. Münch, M. Ise, T. He and A. Fuchs, *Berichte der Bunsen-Gesellschaft*, 1997, **101**, 1344–1350.

[60] P. Berger, F. Mauvy, J. Grenier, N. Sata, A. Magrasó, R. Haugsrud and P. Slatere, in *Proton-Conducting Ceramics*, Pan Stanford, 2015, pp. 24–95.

[61] G. Marnellos, C. Athanasiou and M. Stoukides, *Evaluation and use of the Pd — SrCe0.95Yb0.05O3— Pd electrochemical reactor for equilibrium-limited hydrogenation reactions*, 1-2, 1998.

[62] S. Zisekas, G. Karagiannakis, G. Marnellos and M. Stoukides, *Ionics*, 2002, **8**, 118–122.

[63] X. T. L. SU, R. Quan and J. D. WANG, *Acta Chimica Sinica*, 2003, **4**, year.

[64] Y. Guo, B. Liu, Q. Yang, C. Chen, W. Wang and G. Ma, *Electrochemistry Communications*, 2009, **11**, 153–156.

[65] Y. H. Xie, J. D. Wang, R. Q. Liu, X. T. Su, Z. P. Sun and Z. J. Li, *Solid State Ionics*, 2004, **168**, 117–121.

[66] B. H. Wang, J. De Wang, R. Liu, Y. H. Xie and Z. J. Li, *Journal of Solid State Electrochemistry*, 2005, **11**, 27–31.

[67] B. Wang, R. Liu, J. Wang, Z. Li and Y. Xie, *Chinese Journal of inorganic chemistry*, 2005, **21**, 1551–1555.

[68] I. A. Amar, R. Lan, C. T. Petit, V. Arrighi and S. Tao, *Solid State Ionics*, 2011, **182**, 133–138.

[69] G. J. JANZ and M. R. LORENZ, *Journal of chemical and Engineering data*, 1961, **6**, 321–323.

[70] G. Xu, R. Liu and J. Wang, *Science in China, Series B: Chemistry*, 2009, **52**, 1171–1175.

[71] V. Kordali, G. Kyriacou and C. Lambrou, *Chemical Communications*, 2000, 1673–1674.

[72] Y. Ren, C. Yu, X. Tan, X. Han, H. Huang, H. Huang and J. Qiu, *Small Methods*, 2019, **3**, year.

[73] H. Li, C. Chen, D. Yan, Y. Wang, R. Chen, Y. Zou and S. Wang, 2019.

[74] C. Duan, J. Tong, M. Shang, S. Nikodemski, M. Sanders, S. Ricote, A. Almansoori and R. O'Hayre, *Science*, 2015, **349**, 1321–1326.

[75] E. D. Wachsman and K. T. Lee, *Science*, 2011, **334**, 935–939.

[76] K. S. Lee, S. Maurya, Y. S. Kim, C. R. Kreller, M. S. Wilson, D. Larsen, S. E. Elangovan and R. Mukundan, *Energy and Environmental Science*, 2018, **11**, 979–987.

[77] A. Skodra and M. Stoukides, *Solid State Ionics*, 2009, **180**, 1332–1336.

[78] H. Jeoung, J. N. Kim, C. Y. Yoo, J. H. Joo, J. H. Yu, K. C. Song, M. Sharma and H. C. Yoon, *Korean Chemical Engineering Research*, 2014, **52**, 58–62.

[79] R. Q. Liu, Y. H. Xie, J. D. Wang, Z. J. Li and B. H. Wang, *Solid State Ionics*, 2006, **177**, 73–76.

[80] A. R. Singh, B. A. Rohr, M. J. Statt, J. A. Schwalbe, M. Cargnello and J. K. Nørskov, *ACS Catalysis*, 2019, **9**, 8316–8324.

[81] J. Fleig and J. Maier, *The impedance of ceramics with highly resistive grain boundaries: Validity and limits of the brick layer model*, 6-7, 1999.

[82] A. Skodra and M. Stoukides, *Solid State Ionics*, 2009, **180**, 1332–1336.

[83] D. S. Yun, J. H. Joo, J. H. Yu, H. C. Yoon, J. N. Kim and C. Y. Yoo, *Journal of Power Sources*, 2015, **284**, 245–251.

[84] R. Lan, K. A. Alkhazmi, I. A. Amar and S. Tao, *Applied Catalysis B: Environmental*, 2014, **152-153**, 212–217.

[85] R. Lan, K. A. Alkhazmi, I. A. Amar and S. Tao, *Electrochimica Acta*, 2014, **123**, 582–587.

[86] I. V. Yentekakis, M. Konsolakis, R. M. Lambert, N. MacLeod and L. Nalbantian, *Applied Catalysis B: Environmental*, 1999, **22**, 123–133.

[87] F. Dorado, A. de Lucas-Consuegra, P. Vernoux and J. L. Valverde, *Applied Catalysis B: Environmental*, 2007, **73**, 42–50.

[88] R. M. Lambert, M. Tikhov, A. Palermo, I. V. Yentekakis and C. G. Vayenas, *Ionics*, 1995, **1**, 366–376.

[89] S. Ladas, S. Bebelis and C. G. Vayenas, *Surface Science*, 1991, **251-252**, 1062–1068.

[90] C. G. Vayenas and S. Brosda, *Topics in Catalysis*, 2014, **57**, 1287–1301.

[91] C. G. Vayenas, S. Bebelis, I. V. Yentekakis and S. Neophytides, *Non-Faradaic electrochemical modification of catalytic activity: the work function of metal electrodes in solid electrolyte cells*, PART 1, 1992.

[92] J. H. Koh, N. Weber and A. V. Virkar, *Solid State Ionics*, 2012, **220**, 32–38.

[93] S. N. Heavens, L. Gb, J. S. Blackburn, W. Gb and I. W. Jones, 2013, **2**, year.

[94] Z. Liu, J. Chen, X. Wang, Y. Wang, D. Wang and Z. Mao, *Journal of Materials Science: Materials in Electronics*, 2020.

[95] J. Díez-Ramírez, V. Kyriakou, I. Garagounis, A. Vourros, E. Vasileiou, P. Sánchez, F. Dorado and M. Stoukides, *ACS Sustainable Chemistry and Engineering*, 2017, **5**, 8844–8851.

[96] J. Murakami, M. Futamata, Y. Nakao, S. Horiuchi, K. Bando, U. Nagashima and K. Yoshimura, *Chemical Physics Letters*, 2015, **618**, 1–5.

[97] M. B. Dixit, W. Zaman, Y. Bootwala, Y. Zheng, M. C. Hatzell and K. B. Hatzell, *ACS applied materials & interfaces*, 2019, **11**, 45087–45097.

[98] K. B. Hatzell and Y. Zheng, *MRS Energy & Sustainability*, 2021, 1–7.

[99] C. J. Van Der Ham, M. T. Koper and D. G. Hetterscheid, *Challenges in reduction of dinitrogen by proton and electron transfer*, 2014.

[100] K. Li, S. G. Shapel, D. Hochfilzer, J. B. Pedersen, K. Krempl, S. Z. Andersen, R. Sažinas, M. Saccoccio, S. Li, D. Chakraborty, J. Kibsgaard, P. C. Vesborg, J. K. Nørskov and I. Chorkendorff, *ACS Energy Letters*, 2022, **7**, 36–41.

[101] Z. Zhang, Y. Zhao, B. Sun, J. Xu, Q. Jin, H. Lu, N. Lyu, Z. M. Dang and Y. Jin, *ACS Applied Materials and Interfaces*, 2022.

[102] C. Lv, L. Zhong, Y. Yao, D. Liu, Y. Kong, X. Jin, Z. Fang, W. Xu, C. Yan, K. N. Dinh, M. Shao, L. Song, G. Chen, S. Li, Q. Yan and G. Yu, *Chem*, 2020, **6**, 2690–2702.

[103] Y. Abghoui and E. Skúlasson, *Procedia Computer Science*, 2015, **51**, 1897–1906.

[104] X. Yang, J. Nash, J. Anibal, M. Dunwell, S. Kattel, E. Stavitski, K. Attenkofer, J. G. Chen, Y. Yan and B. Xu, *Journal of the American Chemical Society*, 2018, **140**, 13387–13391.

[105] R. Zhang, H. Guo, L. Yang, Y. Wang, Z. Niu, H. Huang, H. Chen, L. Xia, T. Li, X. Shi, X. Sun, B. Li and Q. Liu, *ChemElectroChem*, 2019, **6**, 1014–1018.

[106] N. Wang, Q. S. Song, W. J. Liu and J. Zhang, *Frontiers in Energy Research*, 2020, **8**, year.

[107] R. Zhang, J. Han, B. Zheng, X. Shi, A. M. Asiri and X. Sun, *Inorganic Chemistry Frontiers*, 2019, **6**, 391–395.

[108] Z. Shao, X. Cao, H. Luo and P. Jin, *NPG Asia Materials*, 2018, **10**, 581–605.

[109] Y. Lee, S. W. Jung, S. H. Park, J. W. Yoo and J. Park, *Materials*, 2020, **13**, 1–13.

[110] S. Ji, Y. Zhao, F. Zhang and P. Jin, *Journal of the Ceramic Society of Japan*, 2010, **118**, 867–871.

[111] A. Chippindale, P. Dickens and A. Powell, *Journal of Solid State Chemistry*, 1991, **93**, 526–533.

[112] Y. Filinchuk, N. A. Tumanov, V. Ban, H. Ji, J. Wei, M. W. Swift, A. H. Nevidomskyy and D. Natelson, *Journal of the American Chemical Society*, 2014, **136**, 8100–8109.

[113] Y. Chen, Z. Wang, S. Chen, H. Ren, L. Wang, G. Zhang, Y. Lu, J. Jiang, C. Zou and Y. Luo, *Nature Communications*, 2018, **9**, 1–8.

[114] Y. Chen, Z. Shao, Y. Yang, S. Zhao, Y. Tao, H. Yao, H. Luo, X. Cao and P. Jin, *ACS Applied Materials and Interfaces*, 2019, **11**, 41229–41237.

[115] L. Fan, Y. Zhu, C. Chen, L. Zhu, B. Wang and Q. Zhang, *The Journal of Physical Chemistry C*, 2022, **126**, 5004–5013.

[116] N. Li, M. Zheng, H. Lu, Z. Hu, C. Shen, X. Chang, G. Ji, J. Cao and Y. Shi, *Chemical Communications*, 2012, **48**, 4106–4108.

[117] H.-C. Tao, L.-Z. Fan, Y. Mei and X. Qu, *Electrochemistry Communications*, 2011, **13**, 1332–1335.

[118] X. Zhu, Y. Zhu, S. Murali, M. D. Stoller and R. S. Ruoff, *ACS nano*, 2011, **5**, 3333–3338.

[119] A. M. Elshurafa, M. N. Almadhoun, K. Salama and H. Alshareef, *Applied Physics Letters*, 2013, **102**, 232901.

[120] Y. Li, K. Sheng, W. Yuan and G. Shi, *Chemical communications*, 2013, **49**, 291–293.

[121] Q. Shou, J. Cheng, L. Zhang, B. J. Nelson and X. Zhang, *Journal of Solid State Chemistry*, 2012, **185**, 191–197.

[122] L. Li, M. Chen, G. Huang, N. Yang, L. Zhang, H. Wang, Y. Liu, W. Wang and J. Gao, *Journal of Power Sources*, 2014, **263**, 13–21.

[123] R. Zhou, Y. Zheng, D. Hulicova-Jurcakova and S. Z. Qiao, *Journal of Materials Chemistry A*, 2013, **1**, 13179–13185.

[124] A. Dutta and J. Ouyang, *ACS Catalysis*, 2015, **5**, 1371–1380.

[125] P. Huang, Z. Cheng, L. Zeng, J. Yu, L. Tan, P. Mohapatra, L.-S. Fan and Y. Zhu, *ACS Catalysis*, 2020, **10**, 14928–14935.

[126] J.-Y. Kim, K.-H. Kim, S.-B. Yoon, H.-K. Kim, S.-H. Park and K.-B. Kim, *Nanoscale*, 2013, **5**, 6804–6811.

[127] Ü. Alver and A. Tanrıverdi, *Applied Surface Science*, 2016, **378**, 368–374.

[128] H. M. El-Bery, Y. Matsushita and A. Abdel-moneim, *Applied Surface Science*, 2017, **423**, 185–196.

[129] V. B. Mohan, R. Brown, K. Jayaraman and D. Bhattacharyya, *Materials Science and Engineering: B*, 2015, **193**, 49–60.

[130] H. Jindal, A. S. Oberoi, I. S. Sandhu, M. Chitkara and B. Singh, *International Journal of Energy Research*, 2021, **45**, 5815–5826.

[131] M. M. Shi, D. Bao, S. J. Li, B. R. Wulan, J. M. Yan and Q. Jiang, *Advanced Energy Materials*, 2018, **8**, year.

[132] C. Li, Y. Fu, Z. Wu, J. Xia and X. Wang, *Nanoscale*, 2019, **11**, 12997–13006.

[133] A. T. Habte, D. W. Ayele and M. Hu, *Advances in Materials Science and Engineering*, 2019, **2019**, year.

[134] S. Abdolhosseinzadeh, H. Asgharzadeh and H. S. Kim, *Scientific Reports*, 2015, **5**, 1–7.

[135] S. Chen, S. Perathoner, C. Ampelli, C. Mebrahtu, D. Su and G. Centi, *Angewandte Chemie International Edition*, 2017, **56**, 2699–2703.

[136] Y. Sun, S. Ding, C. Zhang, J. Duan and S. Chen, *Journal of Materials Chemistry A*, 2021, **9**, 1603–1609.

[137] S. D. Giri and A. Sarkar, *Journal of The Electrochemical Society*, 2016, **163**, H252–H259.

[138] S. M. Abd el Haleem and B. G. Ateya, *Journal of Electroanalytical Chemistry*, 1981, **117**, 309–319.

[139] H. Kim, Y. S. Chung, T. Kim, H. Yoon, J. G. Sung, H. K. Jung, W. B. Kim, L. B. Sammes and J. S. Chung, *Solid State Ionics*, 2019, **339**, 115010.

[140] N. Lazouski, Z. J. Schiffer, K. Williams and K. Manthiram, *Joule*, 2019, **3**, 1127–1139.

[141] Y. Zhao, R. Shi, X. Bian, C. Zhou, Y. Zhao, S. Zhang, F. Wu, G. I. Waterhouse, L. Z. Wu, C. H. Tung and T. Zhang, *Advanced Science*, 2019, **6**, 1802109.

[142] M. A. Brzezinski, *Marine Chemistry*, 1987, **20**, 277–288.

[143] K. K. Dey, S. Jha, A. Kumar, G. Gupta, A. K. Srivastava and P. P. Ingole, *Electrochimica Acta*, 2019, **312**, 89–99.

[144] L. F. Greenlee, J. N. Renner and S. L. Foster, *ACS Catalysis*, 2018, **8**, 7820–7827.

[145] K. Wang, D. Smith and Y. Zheng, *Carbon Resources Conversion*, 2018, **1**, 2–31.

[146] L. Zhou and C. E. Boyd, *Aquaculture*, 2016, **450**, 187–193.

[147] H. Tao, Z. L. Chen, X. Li, Y. L. Yang and G. B. Li, *Analytica Chimica Acta*, 2008, **615**, 184–190.

[148] H. Wang, J. Jia, P. Song, Q. Wang, D. Li, S. Min, C. Qian, L. Wang, Y. F. Li, C. Ma, T. Wu, J. Yuan, M. Antonietti and G. A. Ozin, *Efficient Electrocatalytic Reduction of CO2 by Nitrogen-Doped Nanoporous Carbon/Carbon Nanotube Membranes: A Step Towards the Electrochemical CO2 Refinery*, 27, 2017.

VANDERBILT
UNIVERSITY